http://doi.org/10.1093/plphys/kiab595 PLANT PHYSIOLOGY 2022: 188: 1563–1585

Plant Physiology®

Research Article

ROOT HAIR DEFECTIVE 2 vesicular delivery to the apical plasma membrane domain during Arabidopsis root hair development

Lenka Kuběnová,[1] Michaela Tichá ,[1] Jozef Šamaj ,[1] and Miroslav Ovečka [1,*,†]

1 Department of Cell Biology, Centre of the Region Haná for Biotechnological and Agricultural Research, Faculty of Science, Palacký University Olomouc, Šlechtitelů 27, 783 71 Olomouc, Czech Republic

*Author for communication: miroslav.ovecka@upol.cz
†Senior author

L.K. and M.T. performed experiments, M.O. evaluated data, L.K. and M.O. wrote the manuscript, and J.Š. edited the manuscript and provided infrastructure and funding.

The author responsible for distributing materials integral to the findings presented in this article according to the policy described in the Instructions for Authors (https://academic.oup.com/plphys/pages/general-instructions) is: Miroslav Ovečka (miroslav.ovecka@upol.cz).

Abstract

Arabidopsis (*Arabidopsis thaliana*) root hairs develop as long tubular extensions from the rootward pole of trichoblasts and exert polarized tip growth. The establishment and maintenance of root hair polarity is a complex process involving the local apical production of reactive oxygen species generated by *A. thaliana* nicotinamide adenine dinucleotide phosphate (NADPH) oxidase respiratory burst oxidase homolog protein C/ROOT HAIR-DEFECTIVE 2 (AtRBOHC/RHD2). Loss-of-function *root hair defective 2* (*rhd2*) mutants have short root hairs that are unable to elongate by tip growth, and this phenotype is fully complemented by GREEN FLUORESCENT PROTEIN (GFP)-RHD2 expressed under the *RHD2* promoter. However, the spatiotemporal mechanism of AtRBOHC/RHD2 subcellular redistribution and delivery to the plasma membrane (PM) during root hair initiation and tip growth are still unclear. Here, we used advanced microscopy for detailed qualitative and quantitative analysis of vesicular compartments containing GFP-RHD2 and characterization of their movements in developing bulges and growing root hairs. These compartments, identified by an independent molecular marker mCherry-VTI12 as the trans-Golgi network (TGN), deliver GFP-RHD2 to the apical PM domain, the extent of which corresponds with the stage of root hair formation. Movements of TGN/early endosomes, but not late endosomes, were affected in the bulging domains of the *rhd2-1* mutant. Finally, we revealed that structural sterols might be involved in the accumulation, docking, and incorporation of TGN compartments containing GFP-RHD2 to the apical PM of root hairs. These results help in clarifying the mechanism of polarized AtRBOHC/RHD2 targeting, maintenance, and recycling at the apical PM domain, coordinated with different developmental stages of root hair initiation and growth.

Introduction

Root hairs are specialized lateral tubular extensions of root epidermal cells called trichoblasts. Although their presence is dispensable for plant survival, they considerably increase root surface area, and are involved in effective water and nutrient uptake, which is important for sustained plant growth. Moreover, root hairs represent an excellent and easily accessible model of polar cell expansion in plants because of their position at the root surface, simple structure, and fast growth. Root hair development starts with bulging at

Received September 13, 2021. Accepted November 26, 2021. Advance access publication January 5, 2022

the outer tangential cell wall/plasma membrane (PM) domain in the rootward pole of the trichoblasts, followed by a subsequent transition to tip growth, which is polar expansion at the tip, ensuring the formation of long tubular root hair (Carol and Dolan, 2002; Grierson and Schiefelbein, 2002).

Root hair tip growth is caused by the establishment and maintenance of cellular polarity since it requires polarization of the cytoskeleton, membrane trafficking, and localized cell wall deposition (Šamaj et al., 2006). A tip-focused gradient of calcium (Ca^{2+}) ions also plays a substantial role in all tip-growing cells, including root hairs. Hyperpolarization-activated cation channels maintain an increase in cytosolic Ca^{2+} concentration in the growing tip, transporting apoplastic Ca^{2+} ions inwardly across the PM (Kiegle et al., 2000; Véry and Davies, 2000; Miedema et al., 2001). This tip-focused cytosolic Ca^{2+} gradient is established upon root hair tip growth initiation and persists until its cessation (Dolan et al., 1994; Wymer et al., 1997; Foreman et al., 2003). Other components of the tip growth mechanism are reactive oxygen species (ROS), which are recognized by Ca^{2+} channels and gate their opening. These ROS are generated by the NADPH oxidase RESPIRATORY BURST OXIDASE HOMOLOG PROTEIN C (RBOHC), which is encoded by the *RBOHC/ROOT HAIR DEFECTIVE 2* (*RHD2*) locus in Arabidopsis (*Arabidopsis thaliana*; Foreman et al., 2003). The genome of *A. thaliana* encodes 10 different RBOH members (RBOHA to RBOHJ; Torres et al., 2002; Sagi and Fluhr, 2006). Nevertheless, among all RBOH family members, only AtRBOHC/RHD2 is required to regulate the early stages of root hair tip growth. Mutations in *RBOHH* and *RBOHJ* lead to defects in root hair elongation (Mangano et al., 2017). Although the root hairs of these mutants were shorter than those of the wild-type, they were considerably longer compared to loss-of-function mutants in *RBOHC*. Moreover, the most substantial defects in *rbohh* and *rbohj* mutants are caused by disturbed pollen tube elongation, leading to reduced mutant fertility (Kaya et al., 2019; Zhou et al., 2020).

RHD2 transcription is activated in cells of the root epidermis of diverse root zones from the proximal meristem to the elongation zone (Foreman et al., 2003). Loss-of-function mutations in the *AtRBOHC/RHD2* locus in *rhd2* mutants resulted in short root hairs with missing tip-focused ROS and Ca^{2+} gradients (Schiefelbein and Somerville, 1990; Foreman et al., 2003). Importantly, root hair tip growth of *rhd2-1* mutant can be partly restored by external applications of ROS or by pH alkalization that reinstates the PM activity of Ca^{2+} channels (Monshausen et al., 2007). This indicates positive feedback between apical localization and activity of RHD2, ROS, and Ca^{2+} gradients, controlling root hair development (Foreman et al., 2003; Carol et al., 2005). A fully complemented phenotype of *rhd2* mutants with rescued root hair development has been achieved after transformation with GREEN FLUORESCENT PROTEIN (GFP)-tagged functional AtRBOHC (GFP-RHD2) under the control of its native promoter (Takeda et al., 2008). Tissue- and cell-specific localization studies revealed that GFP-RHD2 signals, particularly in trichoblasts, accumulate in the bulges and apices of growing root hairs (Takeda et al., 2008).

Root hair growth and development are supported by dynamic vesicular trafficking. The apical zone of growing root hairs is enriched with secretory and endocytic/recycling vesicles, balancing macromolecule supply, retrieval, and recycling (Cole and Fowler, 2006; Šamaj et al., 2006; Campanoni and Blatt, 2007). Endosomal compartments represent endomembrane trafficking hubs categorized into early endosomes/trans-Golgi networks (TGNs) and late endosomes/multivesicular bodies (Reyes et al., 2011). Furthermore, early endosomal/TGN compartments merge secretory and endocytic pathways (Viotti et al., 2010; Contento and Bassham, 2012; Qi and Zheng, 2013), and late endosomes/multivesicular bodies are involved in transport pathways toward vacuoles (Bottanelli et al., 2011; Contento and Bassham, 2012). Rab guanosine triphosphatases (GTPases) in the clear zone of root hairs spatiotemporally organize vesicular trafficking, exocytosis, endocytosis, and membrane recycling (Voigt et al., 2005; Berson et al., 2014).

FM dyes allow the fluorescence labeling of PM, highly dynamic populations of early, recycling, and late endosomes in root hairs (Ovečka et al., 2005). Detailed analysis and characterization of distinct endosomal compartments have been achieved using protein markers translationally fused to fluorescent proteins; early endosomal/TGN compartments were specifically detected by Rab GTPase Homolog A1d (RabA1d) and Vesicle transport v-SNARE 12 (VTI12), a **S**oluble **N**-ethylmaleimide-sensitive fusion protein **A**ttachment protein **RE**ceptor (SNARE) protein (Sanderfoot et al., 2001; Uemura et al., 2004; Ovečka et al., 2010; Berson et al., 2014). A molecular marker based on the FYVE domain (a zinc finger domain named according to the four cysteine-rich proteins: **F**ab 1, yeast ortholog of PIKfyve, **Y**OTB, **V**ac 1, vesicle transport protein, and **E**EA1, in which it has been found), specifically binding to phosphoinositol-3-phosphate, was used to detect late endosomes (Gillooly et al., 2001; Voigt et al., 2005). Members of the Rab-GTPase family, including RabF2a, RabF1 (Ueda et al., 2004; Voigt et al., 2005; Haas et al., 2007), and RabF2b (Geldner et al., 2009), have been verified as markers for late endosomal compartments and eventually colocalize with FYVE. The dynamic properties of early and late endosomes using molecular markers have been described in the growing root hairs of Arabidopsis (von Wangenheim et al., 2016).

Structural sterols modulate the permeability and fluidity of plant membranes and influence the physical and physiological properties of membrane proteins (Mukherjee and Maxfield, 2000; Clouse, 2002). They play important roles in vesicle trafficking and docking, signaling, and protein localization in membranes (Lindsey et al., 2003), particularly in root hairs (Ovečka et al., 2010) and pollen tubes (Liu et al., 2009). Sterols interact with phospholipids and create macromolecular nanodomains in the extracellular leaflet of the PM, so-called "lipid rafts" (Simons and Toomre, 2000).

Lipid rafts are involved in perceiving and transduction of signals associated with membrane receptors, selecting exo-endocytic cargo molecules, and intracellular redistribution of sterols (Menon, 2002). Proteomic studies identified NADPH oxidases NtRBOHD, StRBOHB, and AtRBOHB with other PM proteins enriched in the detergent-resistant membrane fraction of suspension cells (Morel et al., 2006; Srivastava et al., 2013). Subcellular visualization revealed AtRBOHD localization to dynamic spots at the PM and its endocytosis induced by salt stress (Hao et al., 2014). Nevertheless, the spatiotemporal relationship between local arrangements of structural sterols and integral PM proteins such as AtRBOHC/RHD2 during root hair development is still unclear.

This study examined the qualitative and quantitative localization patterns of GFP-RHD2 during root hair formation in Arabidopsis using advanced microscopy methods. We revealed that incorporating GFP-RHD2 into the apical and subapical PM domains tightly corresponded with the establishment of the apical zone in bulges and growing root hairs. We documented the delivery of GFP-RHD2 to the apical zone during bulge formation and the apex of growing root hairs by dynamic vesicular compartments. These were identified as early endosomal/TGN compartments using colocalization analyses with reliable endosomal molecular markers. Single-particle tracking analysis revealed complex movement patterns of vesicular compartments containing GFP-RHD2 and identified their interactions with the apical PM during root hair formation. In addition, we revealed the possible involvement of structural sterols in the accumulation, docking, and incorporation of GFP-RHD2 vesicles at the apical PM domain of root hairs. Consequently, the genetic approach showed that early endosomal/TGN compartments were more seriously affected in their movements than late endosomes in the *rhd2-1* mutant. This quantitative advanced microscopy study demonstrated the complex nature of GFP-RHD2 delivery, maintenance, and recycling at the apical PM, during root hair formation in Arabidopsis.

Results

Cell type-specific and subcellular distribution patterns of GFP-RHD2 in Arabidopsis root

Light-sheet fluorescence microscopy (LSFM) provided visualization for developmentally regulated and cell type-specific distribution patterns of GFP-RHD2 in growing Arabidopsis roots. The GFP-RHD2 signal was observed in epidermal cells in root hair formation zone, and was explicitly accumulated in the bulges and apices of developing root hairs (Figure 1A). Orthogonal projections from different root developmental zones confirmed GFP-RHD2 localization in the root epidermis, preferably in trichoblasts within the root differentiation and elongation zone (Figure 1B). Specifically, GFP-RHD2 accumulated at the tips of emerging (Figure 1, A and C) and growing (Figure 1, A and D) root hairs. This distribution and accumulation pattern of GFP-RHD2 was confirmed by a pseudo-color-coded, semi-quantitative fluorescence intensity evaluation for maximum intensity projections of the whole root apex (Figure 1A; Supplemental Movie S1) and orthogonal projections of different root developmental zones (Figure 1, B–D). Advanced cellular and sub-cellular localization of GFP-RHD2 using Airyscan confocal laser scanning microscopy (CLSM) revealed a differential abundance of GFP-RHD2 in

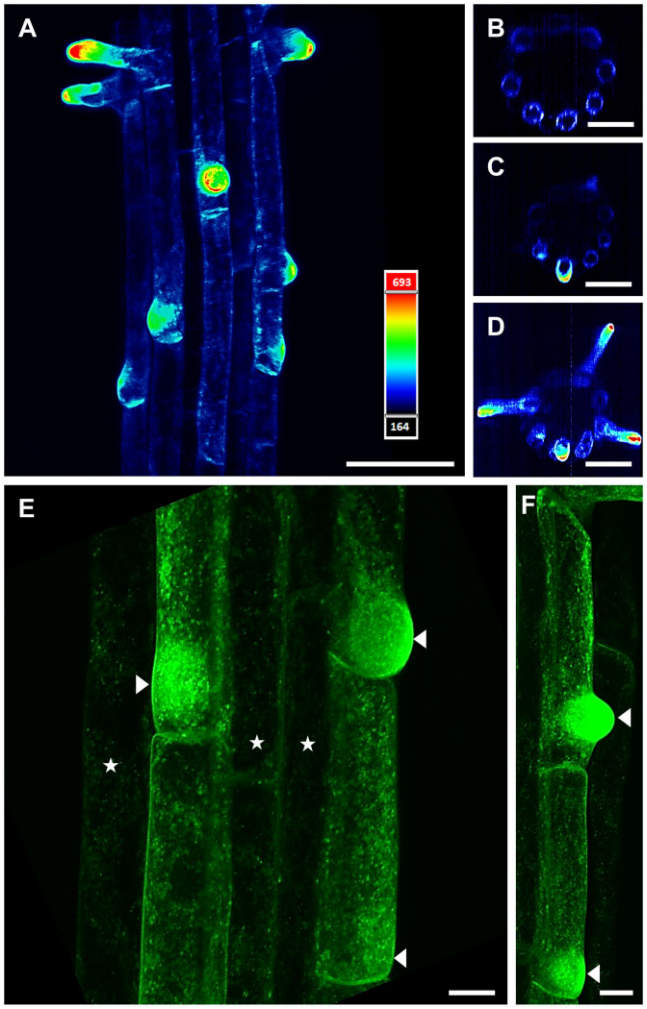

Figure 1 Expression pattern and cell type-specific distribution of GFP-RHD2 in growing Arabidopsis root. A–D, Distribution pattern in root hair formation zone (A), where GFP-RHD2 was expressed mainly in trichoblasts (B) and accumulated at tips of emerging (C) and growing (D) root hairs. Maximum intensity projection of the root hair formation zone (A) and orthogonal projections at different developmental root zones (B–D) from LSFM imaging as visualized using semi-quantitative fluorescence intensity distribution and pseudo-color-coded scale, where dark blue represents minimal intensity (164 arbitrary units) and pale red represents maximum intensity (693 arbitrary units). Spatial overview of the maximum intensity projection from the root hair formation zone (A) is presented in Supplemental Movie S1. E and F, Detailed visualization of subcellular compartments containing GFP-RHD2 in trichoblasts and their progressive accumulation in developing bulges (arrowheads) using Airyscan CLSM. A substantially lower number of compartments with GFP-RHD2 was detected in atrichoblasts (asterisks). Scale bar = 50 μm (A), 40 μm (B–D), 10 μm (E and F).

trichoblasts and atrichoblasts (Figure 1E) as well as specific enrichment in bulge selection sites and developing bulges of trichoblasts (Figure 1, E and F). Most importantly, Airyscan CLSM imaging revealed GFP-RHD2 presence in small motile compartments in the cytoplasm (Figure 1, E and F). Their number was considerably higher in trichoblasts (Figure 1E), and there was an apparent progressive accumulation in developing bulges (arrowhead in Figure 1, E and F). In addition to the visualization of GFP-RHD2 in small compartments in the cytoplasm, Airyscan CLSM revealed localization in the PM, particularly at bulging sites and apical domains of developing bulges (Figure 1, E and F).

We used time-lapse imaging of dynamic GFP-RHD2 localization and targeted accumulation during root hair formation to present the whole dynamic process in the form of a video. The localization pattern of GFP-RHD2 can be related to the root hair growth rate, which is known to change in diverse root hair developmental stages. Time-lapse recording (Supplemental Movie S2) allowed identification of particular stages from early bulges (Stage I; Figure 2A) to late bulges (Stage II; Figure 2B) at the beginning, followed by stages of accelerated root hair tip growth. Subsequent developmental stages were represented by short root hairs (Stage III; Figure 2C), a transition from short to long root hairs (Stages III and IV; Figure 2D), and long root hairs (Stage IV; Figure 2E). The pattern of the tip growth rate over the entire process was quantitatively analyzed using kymographs. In the long-term time-lapse acquisition set up, which was based on recording every 5 min (Figure 2, A–E; Supplemental Movie S2), we recorded a slow extension in early bulges (Stage I) and a faster extension in late bulges (Stage II; Supplemental Figure S1, A and B), followed by fast, smooth, and continuous tip growth of short and long root hairs (Stages III and IV; Supplemental Figure S1 C–F). Nongrowing root hairs (Supplemental Figure S1G) were also identified using this method (Supplemental Figure S1H). The slow mode of the bulge extension versus the fast mode of the root hair extension and particularly sustained regular mode of tip growth in short and long root hair stages were revealed (Figure 2F). Sub-cellular time-lapse imaging of GFP-RHD2 distribution at different stages of root hair initiation showed polarized accumulation at the bulging sites and emerging bulges. GFP-RHD2-positive compartments were mainly enriched in the cortical cytoplasm of the bulging domain and selectively targeted to the apical PM of the emerging bulge (Figure 2G). Polarized accumulation of GFP-RHD2 at the apical PM was documented in the late bulges (Figure 2, H and I; Supplemental Movie S3), short (Figure 2, J and K; Supplemental Movie S4), and long (Figure 2, L and M; Supplemental Movie S5) growing root hairs. GFP-RHD2 at the apical PM was also temporarily maintained in growth-terminating root hairs (Figure 2, N and O; Supplemental Movie S6). Importantly, GFP-RHD2 was present in the cortical cytoplasm of developing bulges (Figure 2, H and I; Supplemental Movie S3) and accumulated in the apical, vesicle-rich "clear" zone of tip-growing root hairs (Figure 2, J–M; Supplemental Movies S4 and S5). Thus, GFP-RHD2 accumulation in PM was detected only in specific domains of the trichoblast, bulging out of the parental outer tangential PM during bulge formation (Figure 2, A and B) and in the apex of growing root hairs (Figure 2, C–E; Supplemental Movie S2). Live cell imaging revealed the presence of GFP-RHD2 in small compartments of the cortical cytoplasm (Figure 2G) and targeted GFP-RHD2 accumulation in the apical PM. Visualization of GFP-RHD2 distribution in growing root hairs, both at early (Figure 2, J and K) and later (Figure 2, L and M) stages, showed an accumulation of GFP-RHD2 in the apical PM, and in compartments in the clear zone, and subapical cytoplasm. Similarly, the PM specifically accumulated GFP-RHD2 only within the apical and subapical zones of root hairs (Figure 2, J–M; Supplemental Figure S1, C and E).

Localization analysis showed a different range of GFP-RHD2 specific targeting to the apical PM domain at distinct stages of root hair development. Therefore, we analyzed the range of PM decorated with GFP-RHD2 (Figure 3A). A quantitative evaluation revealed that the extent of the PM zone containing GFP-RHD2 increased progressively from early to late bulges. This zone was enlarged in short growing root hairs and reached a maximum in longer growing root hairs but declined considerably in nongrowing root hairs (Figure 3B). Thus, the distribution pattern of GFP-RHD2 at the apical PM was tightly associated with the individual developmental stages of root hairs (Figure 3, A and B). The GFP-RHD2 fluorescence signal intensity distribution further corroborated this finding. Visualization using the semi-quantitative 2.5-D rendering function demonstrated a gradual increase in GFP-RHD2 fluorescence signal intensity in successive root hair developmental stages, from the development of the early bulge up to fast-growing root hairs (Supplemental Figure S2).

Live cell imaging revealed targeted delivery of GFP-RHD2 in dynamic vesicular compartments to the cortical cytoplasm and apical PM of developing root hairs. Based on the nature of their movements, we determined three groups of vesicular compartments carrying GFP-RHD2. The first group was represented by compartments with targeted movement to the apical PM. The second group consisted of compartments moving in the cytoplasm without any contact with the apical PM. The third group of compartments moved toward the PM and subsequently moved back to the cytoplasm after making contact. The quantitative evaluation showed a high proportion of GFP-RHD2 vesicular compartments moving toward the apical PM. A low number of compartments moved without contact or moved back after contact with the PM in the early bulge stage (Figure 3C). However, this turned to a different pattern during root hair development. The proportions of compartments from the first group, with targeted movement to the apical PM, was relatively high in short- and longer growing root hairs, while the compartments from the third group, moving toward the PM and subsequently back to the cytoplasm after

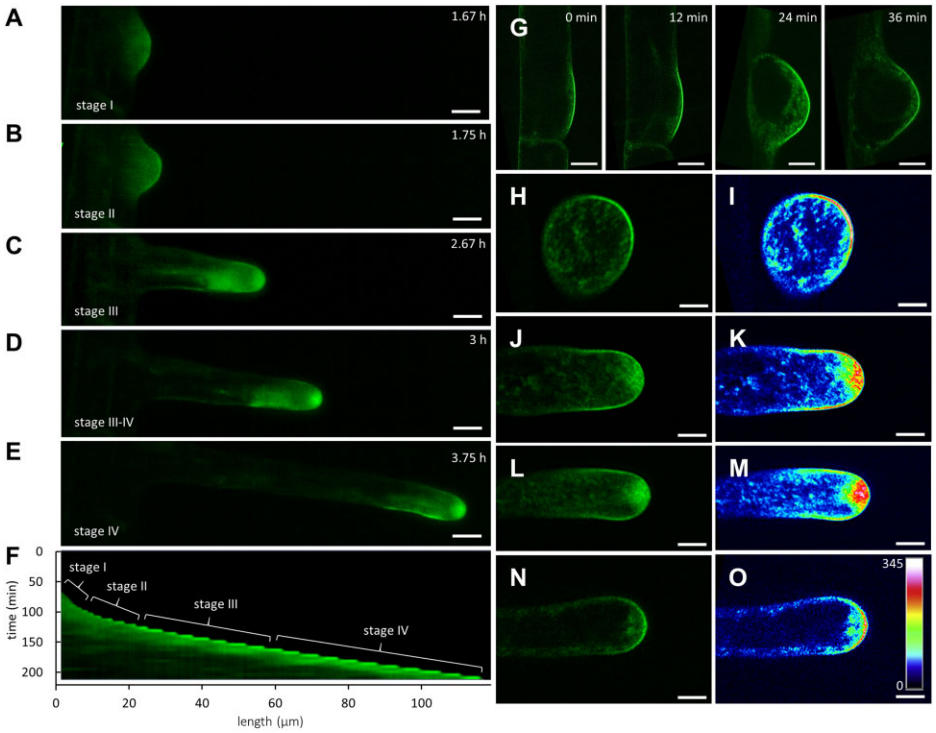

Figure 2 Time-course imaging of GFP-RHD2 localization and accumulation during root hair formation. A–F, Localization pattern of GFP-RHD2 in different stages of root hair development and its relation to the particular root hair growth rate. Time-lapse recording of developing root hair showing stages of the early bulge (A; Stage I), late bulge (B; Stage II), short root hair (C; Stage III), the transition from short to long root hair (D; Stages III and IV), and long root hair (E; Stage IV). The whole process shown in Supplemental Movie S2 is quantitatively presented in kymograph (F), representing the pattern and rate of the growth of this particular root hair, growing over the distance of 120 µm within the time period of 220 min. Individual developmental stages presented in (A–E) are depicted in (F). G, Lateral view on the polarized accumulation of GFP-RHD2 at the PM domain and cortical cytoplasm of the bulging site and during the emerging of the bulge. H–O, The GFP-RHD2 distribution (H, J, L, and N) and a semi-quantitative signal intensity visualization using a pseudo-color-coded range (I, K, M, and O) of the polarized accumulation at the apical PM domain and cortical cytoplasm in the late bulge (H and I; Supplemental Movie S3), short (J and K; Supplemental Movie S4), and longer (L and M; Supplemental Movie S5) growing root hairs, and in nongrowing root hair (N and O; Supplemental Movie S6). The pseudo-color-coded scale ranges from dark blue representing minimal intensity (0 arbitrary units) to white representing maximum intensity (345 arbitrary units). Timing of the sequential imaging is indicated in hours (h) using light-sheet fluorescence microscopy (A–E) and in minutes (min) using Airyscan CLSM (G). Scale bar = 10 µm (A–E), 5 µm (G–O).

making contact, considerably increased (Figure 3C). With the cessation of tip growth, there was a considerable reduction in compartments moving to the apical PM (Figure 3C). This analysis showed that the extent of GFP-RHD2 specifically targeted to the apical PM corresponded with the stages of root hair formation. Importantly, this association was directly affected by the ratio between GFP-RHD2 vesicular compartments targeted to the apical PM and those moving back to the cytoplasm after contacting the PM.

Identification of GFP-RHD2-positive compartments

Next, we analyzed the nature of compartments containing GFP-RHD2 by colocalization with the selective membrane styryl dye FM4–64. In root hairs, the FM4–64 dye is able to stain the PM and early endocytotic/recycling vesicular compartments after a minute-long exposure period (Ovečka et al., 2005). After 10 min of application, FM4–64 colocalized with GFP-RHD2 at the PM and in motile vesicular compartments in the apical and subapical zones of growing root hairs (Figure 4A). The colocalization at PM was semi-quantitatively documented by a cross-sectional fluorescence intensity profile measurement within the subapical zone of the root hair (Figure 4B). A high degree of colocalization in moving vesicular compartments within the subapical zone of growing root hairs (Figure 4C) was revealed by fluorescence intensity profile measurements (Figure 4D). Semi-quantitative measurement of fluorescence signal intensities of GFP-RHD2 and FM4–64 at the PM along the whole longitudinal root hair axis showed a stable level of FM4–64 fluorescence in the subapical and shank regions, but GFP-RHD2 fluorescence was specifically enriched only in the apical and subapical PM domains and gradually decreased in the shank region (Figure 4E). The quantitative colocalization analysis corroborated the results from semi-quantitative profile measurements showing a high degree of Pearson's correlation coefficients between FM4–64 and GFP-RHD2 in intracellular compartments (Figure 4F; Supplemental Figure S3, A and B) and in the subapical PM (Figure 4G;

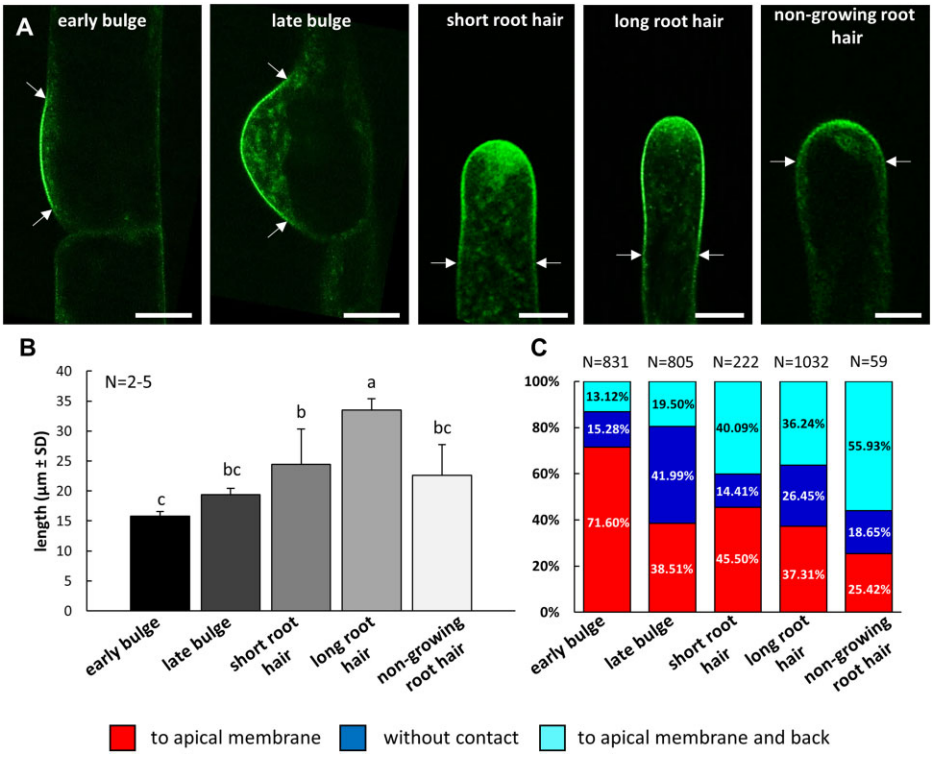

Figure 3 Determination of GFP-RHD2 localization at the apical PM domain at different stages of root hair formation and growth. A, Delineation of the area (by two arrows) where GFP-RHD2 was specifically targeted to the apical PM domain at early and late bulging stage, in short and longer growing root hairs, and in nongrowing root hairs. B, Quantitative evaluation of the apical PM domain length decorated by GFP-RHD2 at different stages of root hair development. Measurement was done from 2 to 5 root hairs. Different lowercase letters indicate statistical significance between treatments according to one-way analysis of variance (ANOVA) and subsequent least significant difference (LSD) test ($P < 0.05$). Error bars represent standard deviations. C, Quantitative determination of the ratio between the compartments containing GFP-RHD2 and showing targeted movement to the apical PM (red), moving in the cytoplasm without any contact with the apical PM (blue), or moving to and contacting the PM and subsequently moving back to the cytoplasm (cyan). The GFP-RHD2-positive compartments were tracked and analyzed at denoted stages of root hair development as depicted in (A). More than 59 compartments from 3 to 7 growing root hairs from individual plants were analyzed. Scale bar = 5 µm (A).

Supplemental Figure S3, C and D). This analysis suggests that vesicular compartments containing GFP-RHD2 might belong to the early endosome group.

Transgenic Arabidopsis line carrying GFP-RabA1d marker was used to visualize early endosomal/TGN compartments (Ovečka et al., 2010; Berson et al., 2014; von Wangenheim et al., 2016). Colocalization analysis of GFP-RabA1d with FM4–64 in growing root hairs revealed no overlap at the PM (Supplemental Figure S4, A and C). However, GFP-RabA1d colocalized with FM4–64 (applied for 10 min) in motile compartments (Supplemental Figure S4, E and F). This was corroborated by a quantitative colocalization analysis using Pearson's correlation coefficients, showing high values in intracellular compartments (Figure 4F; Supplemental Figure S5, A and B) and low values in the subapical PM (Figure 4G; Supplemental Figure S5, C and D). RabF2a-YFP is an appropriate marker of late endosomes (von Wangenheim et al., 2016) and colocalization analysis with FM4–64 (applied for 10 min) revealed no colocalization in growing root hairs both at the PM (Supplemental Figure S4, B and D) and in motile compartments (Supplemental Figure S4, G and H). Again, a quantitative colocalization analysis using Pearson's correlation coefficients corroborated this observation, showing very low values both in intracellular compartments (Figure 4F; Supplemental Figure S6, A and B) and in the subapical PM (Figure 4G; Supplemental Figure S6, C and D).

Colocalization analysis using FM4–64 suggested that vesicular compartments delivering GFP-RHD2 toward the apical PM in growing root hairs are likely early endosomes/TGN. To confirm this suggestion, we prepared double transgenic lines carrying GFP-RHD2 together with the early endosomal/TGN marker, mCherry-VTI12, or with the late endosomal marker, mCherry-RabF2b. Markers mCherry-VTI12 and mCherry-RabF2b were not detected in the PM of growing root hairs (Supplemental Figure S7). Therefore, these two markers did not colocalize with GFP-RHD2 at the PM (Figure 5, A–D and J; Supplemental Figures S8, C and D and S9, C and D). However, the early endosomal/TGN marker mCherry-VTI12 showed colocalization with GFP-RHD2 in motile compartments (Figure 5, A and E); this was confirmed by fluorescence intensity profile quantification (Figure 5F) and a quantitative colocalization analysis using Pearson's correlation coefficients (Figure 5I; Supplemental

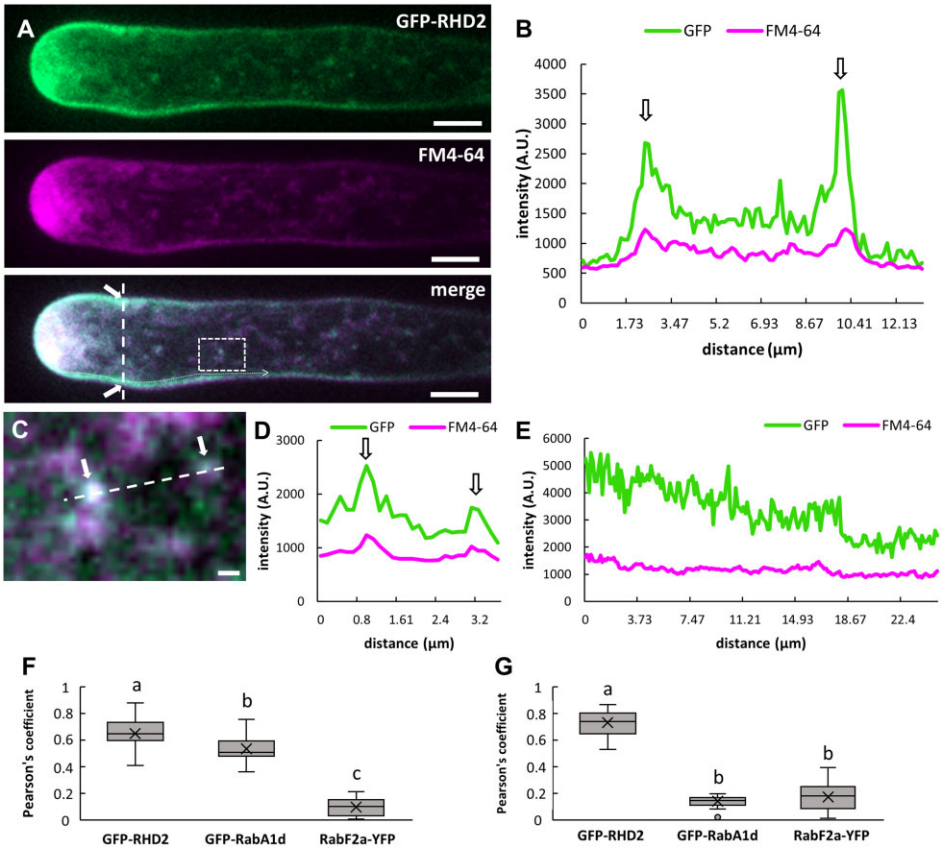

Figure 4 Colocalization analysis of GFP-RHD2 with selective membrane styryl dye FM4–64 in growing root hairs. A, Localization pattern of GFP-RHD2 (green) in the apical PM domain, the cytoplasm of the apical and subapical zone, and in motile compartments of growing root hair co-labeled with membrane styryl dye FM4–64 (magenta). Colocalization analysis has been performed in the merged image along the cross-section profile marked by an interrupted white line (white arrows indicate the PM), in compartments within the white box, and along the white dotted line. B, Fluorescence intensity profile of the GFP and FM4–64 signal measured along the cross-section interrupted white line in (A). Arrows indicate the position of the PM. C, Detailed image of compartments containing GFP-RHD2 and FM4–64 within the white box depicted in (A). Arrows indicate the position of the compartments and the interrupted white line depicts the profile for fluorescence intensity quantification. D, Fluorescence intensity profile of the GFP and FM4–64 signal along the interrupted white line in (C). Arrows indicate the position of the compartments. E, Fluctuation of the GFP and FM4–64 fluorescence signal intensity at the PM along the longitudinal root hair axis from apex to the shank region measured along the white dotted line in (A). Note the stable level of FM4–64 fluorescence signal intensity at the PM in the subapical and shank region, while GFP-RHD2 fluorescence signal intensity was specifically enriched in the apical and subapical PM domains and gradually decreased within the shank region. F and G, Quantitative colocalization analysis using Pearson's correlation coefficients between FM4–64 and GFP-RHD2, early endosomal marker GFP-RabA1d (Supplemental Figure S4A), and late endosomal marker RabF2a-YFP (Supplemental Figure S4B) in intracellular compartments (F), and in subapical PM (G). Three independent ROIs from five individual root hairs at 5 different time points were selected, providing 75 measured vesicular compartments in total from each analyzed time point. Analogously, 25 measurements of PM in total from each time point originating from 5 individual root hairs were analyzed. Box plots display the first and third quartiles, split by the median; the crosses indicate the mean values; whiskers extend to include the max/min values. Different lowercase letters indicate statistical significance between lines according to one-way ANOVA and subsequent LSD test ($P < 0.05$). Selections of ROIs and scatterplots of measurements are presented in Supplemental Figures S3, S5, and S6. Scale bar = 5 µm (A), 1 µm (C).

Figure S8, A and B). Topological colocalization analysis (Figure 5B), fluorescence intensity profile quantification (Figure 5, G and H), and quantitative colocalization analysis using Pearson's correlation coefficients (Figure 5I; Supplemental Figure S9, A and B) suggested no colocalization between GFP-RHD2 and mCherry-RabF2b, which represents marker for late endosomal compartments. Concluding from colocalization results with FM4–64 and endosomal markers, vesicular trafficking and targeted delivery of GFP-RHD2 during root hair development seem to depend on early endosomal/TGN compartments.

Quantitative microscopic analysis of motile compartments containing GFP-RHD2 at different stages of root hair development

Live cell imaging of developing root hairs by advanced microscopy enabled the qualitative determination of

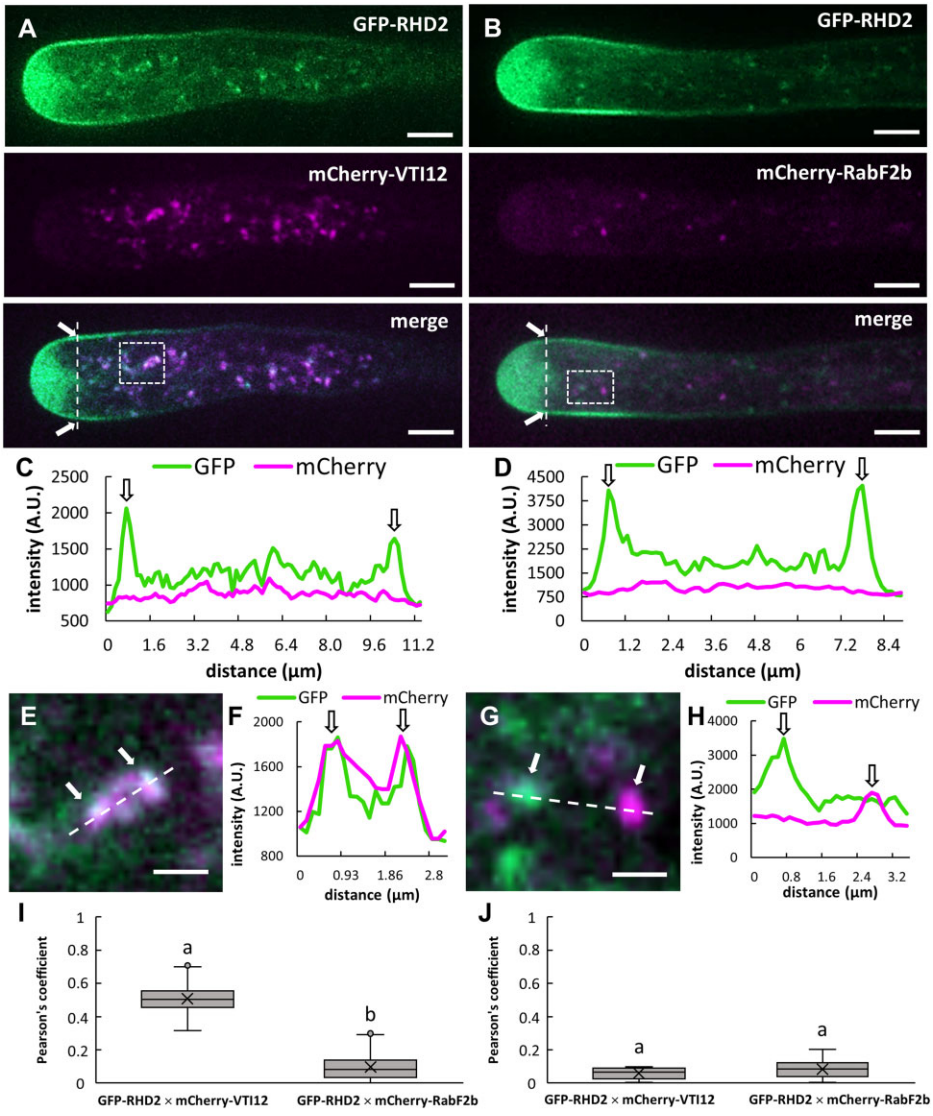

Figure 5 Colocalization analysis of GFP-RHD2 with early and late endosomal markers in growing root hairs. A, Distribution of GFP-RHD2 in the apical PM domain, the clear zone, the cytoplasm of the subapical zone, and in moving compartments of growing root hair of Arabidopsis double transgenic line carrying both GFP-RHD2 (green) and the early endosomal/TGN marker mCherry-VTI12 (magenta). B, Distribution of GFP-RHD2 in the apical PM domain, the clear zone, the cytoplasm of the subapical zone, and in moving compartments of growing root hair of Arabidopsis double transgenic line bearing both GFP-RHD2 (green) and the late endosomal marker mCherry-RabF2b (magenta). In merged images of (A) and (B), an extent of fluorescence intensity colocalization has been analyzed along the cross-section profiles marked by interrupted white lines (white arrows indicate the PM) and in moving compartments within the white boxes. C, Fluorescence intensity profiles of GFP and mCherry signals along the cross-section interrupted the white line of the root hair shown in (A). D, Fluorescence intensity profiles of the GFP and mCherry signal along the cross-section interrupted the white line of the root hair shown in (B). Arrows in (C) and (D) indicate the position of the PM. E, Detailed image of compartments containing GFP-RHD2 and mCherry-VTI12 within the white box in (A). F, Fluorescence intensity profile of the GFP and mCherry-VTI12 signal along the interrupted white line in (E). G, Detailed image of compartments positive to GFP-RHD2 and mCherry-RabF2b within the white box in (B). H, Fluorescence intensity profile of the GFP and mCherry-RabF2b signal along the interrupted white line in (G). Arrows indicate the position of the compartments. I and J, Quantitative colocalization analysis using Pearson's correlation coefficients between GFP-RHD2 and the early endosomal/TGN marker mCherry-VTI12, and between GFP-RHD2 and the late endosomal marker mCherry-RabF2b, in intracellular compartments (I), and in the subapical PM (J). Three independent ROIs from five individual root hairs at five different time points were selected, providing 75 measured vesicular compartments in total per line from each analyzed time point. Analogously, 25 measurements of PM in total per line from each time point originating from five individual root hairs were analyzed. Box plots display the first and third quartiles, split by the median; the crosses indicate the mean values; whiskers extend to include the maximum/minimum values. Different lowercase letters indicate statistical significance between lines according to one-way ANOVA and subsequent LSD test ($P < 0.05$). Selections of ROIs and scatterplots of measurements are presented in Supplemental Figures S8 and S9. Scale bar = 5 µm (A and B), 1 µm (E and G).

compartments containing GFP-RHD2. We analyzed the quantitative parameters of their movements in different stages of root hair formation using the particle-tracking method and characterized three independent groups of the GFP-RHD2 compartments. The first group was marked in red (compartments moving to the apical PM and fusing with it), the second group was marked in blue (compartments moving in the cytoplasm without any contact with the apical PM), and the third group was marked in cyan (compartments moving to and contacting the PM and subsequently moving back to the cytoplasm). Movement distances of GFP-RHD2 compartments during a 60 s period imaged by Airyscan CLSM were tracked using the "tracked cells function" of the ARIVIS Vision4D software. These trajectories were directly displayed in a color-coded mode in the image sequences of early (Figure 6A), and late (Figure 6C) bulges, as well as short (Figure 6E) and longer (Figure 6G) growing root hairs. In addition, the values of the maximum and the average speed of movement were analyzed.

Line tracking trajectories in different stages of root hair development clearly distinguished spatial separation of GFP-RHD2 compartments from different groups (Figure 6, A, C, E, and G). Compartments from the red group were located almost exclusively in the bulging site (Figure 6A) and the whole bulges (Figure 6C) as well as in the clear and subapical zones of growing root hairs (Figure 6, E and G). In contrast, GFP-RHD2 compartments from the cyan group were located mainly at the periphery of the bulging zone (Figure 6A) and developing bulging domains (Figure 6C). In growing root hairs, compartments from the cyan group moved preferably in the subapical and shank regions, contacting the lateral PM (Figure 6, E and G) exclusively. Differences in the spatial distribution of individual

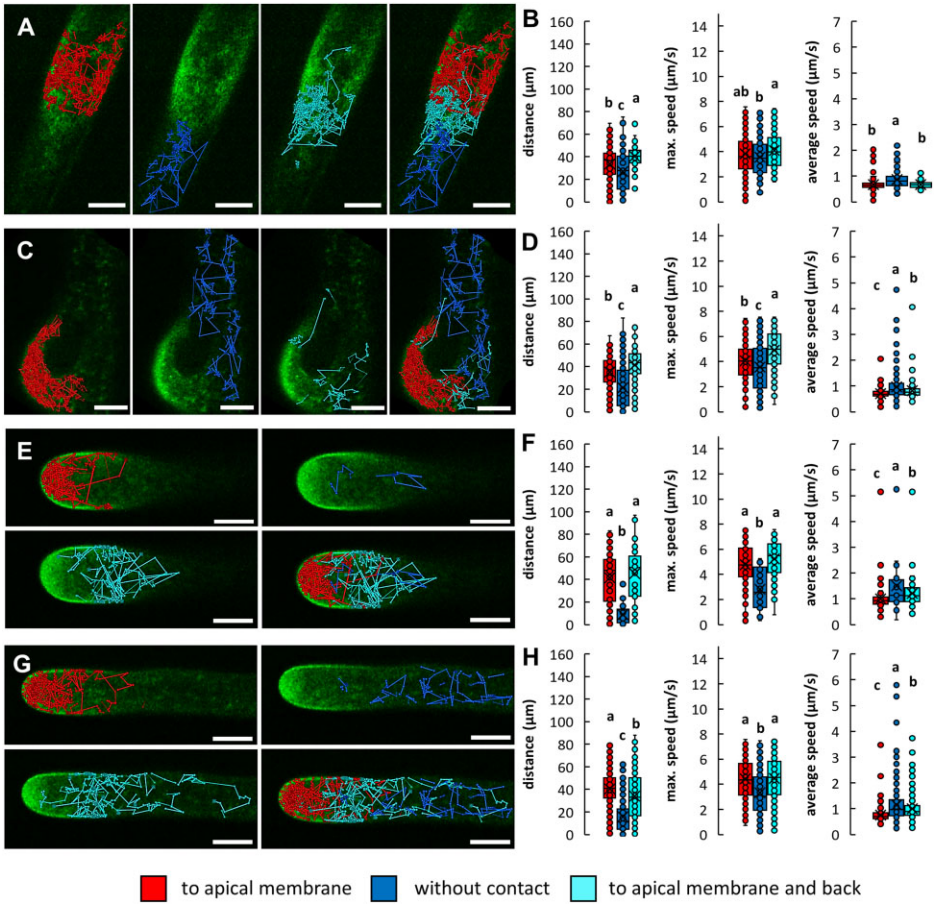

Figure 6 Qualitative determination and quantitative tracking of moving compartments containing GFP-RHD2 at different stages of root hair development. A, C, E, and G, Line tracking of the compartments showing targeted movement to the apical PM (red), moving in the cytoplasm without any contact with the apical PM (blue), and moving to and contacting the PM and moving back to the cytoplasm (cyan), and merged images of all three types of tracks in the early bulge (A), late bulge (C), short (E), and longer (G) growing root hairs. B, D, F, and H, Quantitative determination of tracked distance of compartments, maximum and average speeds of their movements during tracking analysis, as compared separately for the compartments showing targeted movement to the apical PM (red), moving in the cytoplasm without any contact with the apical PM (blue), and moving to and contacting the PM and moving back to the cytoplasm (cyan) in the early bulge (B), late bulge (D), short (F), and longer (H) growing root hairs. More than 222 compartments from 3 to 7 growing root hairs from individual plants were analyzed. Box plots show the first and third quartiles, split by the median (line) and mean (cross). Whiskers extend to include the max/min values. Different lowercase letters indicate statistical significance between treatments according to one-way ANOVA and subsequent LSD test ($P < 0.05$). Scale bar = 5 µm.

compartments might be associated with the distance and speed of movement in different root hair developmental stages. Compartments from the blue group showed the shortest displacement distances in almost all cases (Figure 6, B, D, F, and H; Supplemental Figure S10), with the lowest values in maximum movement speed. However, the average speed of these compartments was the highest (with the highest variability) at all stages of root hair development (Figure 6, B, D, F, and H). Compartments from the red group moved along short distances in early and late bulging stages (Figure 6, B and D). These distances increased significantly during root hair tip growth compared to the cyan group (Figure 6, F and H). Compartments from the cyan group moved over the longest distance in early and late bulging stages (Figure 6, B and D), but these values decreased in the growing root hair stage (Figure 6, F and H; Supplemental Figure S10). The maximum movement speed was comparable between compartments from the red and cyan groups. Still, the average speed was significantly higher in compartments from the cyan group compared to the red group, particularly in growing root hairs (Figure 6, B, D, F, and H). The trend of faster movement of compartments from the cyan group was evident from the frequency distribution graphs. The curves for the maximum speed of cyan group compartments were right-shifted toward higher micrometer per second values (Supplemental Figure S10).

GFP-RHD2 was also localized to motile compartments in atrichoblasts. We carried out a comparative quantitative tracking analysis to characterize their properties with compartments from trichoblasts moving outside the bulging zone (Supplemental Figure S11, A and B). In principle, there were no significant differences in the average distance and minimum/maximum/average movement speed (Supplemental Figure S11, C and D). When the motions and dynamic behavior of compartments containing GFP-RHD2 were compared between tricho and atrichoblasts (Supplemental Figure S11, A and B), those in atrichoblasts showed more variable movement and dynamics. This trend was evident from the frequency distribution graphs, revealing a slightly shifted distribution to longer distances for GFP-RHD2 compartments in trichoblasts (Supplemental Figure S11E). However, the frequency distribution of maximum (Supplemental Figure S11F) and average (Supplemental Figure S11G) movement speed were very similar. These data indicate that trichoblast compartments with GFP-RHD2, which are not involved in root hair formation, move similarly to those from the atrichoblasts but distinctly from those from developing root hairs.

Live-cell imaging using Airyscan CSLM allowed the visualization of close contacts between motile compartments and the apical PM in the root hair and provided substantially improved spatial resolution. Time-course visualization of individual compartments containing GFP-RHD2 revealed direct contact with the PM enriched with GFP-RHD2 (Figure 7A; Supplemental Movie S7). It was possible to document the full incorporation of these compartments into the apical PM by complete fusion (Figure 7, B and D; Supplemental Movie S8). Alternatively, we observed only temporal contacts of such compartments, lasting for ∼30–50 s, but without full integration to the PM (Figure 7, C and E; Supplemental Movie S9). Such docking events without complete incorporation into the PM lasted longer than the total fusion events (cf. Figure 7, B and D to C and E).

Movements of early endosomes/TGN and late endosomes in *rhd2-1* mutant

Colocalization and common characteristics of compartments containing GFP-RHD2 and early endosomes/TGN but not late endosomes (Figures 4 and 5) raised the question of whether endosomal movements are affected in the *rhd2-1* mutant. To address this, we prepared transgenic *rhd2-1* lines carrying the early endosomal/TGN marker GFP-RabA1d and the late endosomal marker RabF2a-YFP. Since the *rhd2-1* mutant only produced short root hairs that were unable to grow, we performed quantitative tracking of endosomal compartments showing targeted movement to the bulge (red group), moving in the cytoplasm outside of the bulge (blue group), and moving toward the bulge and back (cyan group) during a 60 s imaging period. Quantitative determination of the ratio between individual groups revealed a higher proportion of early endosomes/TGN moving to the bulges in the *rhd2-1* mutant (Figure 8A). However, similar to the compartments moving to the bulge and back (the cyan group), the compartments from the red group moved over shorter distances compared to the control line (Figure 8, B–D). Characterization of movement parameters of GFP-RabA1d compartments in the control line by the frequency distribution diagram revealed different behaviors of individual groups (Figure 8, E and F). In particular, the curves for maximum speed were shifted differentially (Figure 8E). This indicates different properties of early endosomal/TGN compartments that participate in bulge formation. In contrast, frequency distribution analysis of the speed among all three different groups of GFP-RabA1d compartments in the *rhd2-1* mutant showed no differences (Figure 8, G and H). These data indicated that the movement of early endosomal/TGN compartments was partially affected in *rhd2-1*.

Late endosomal compartments did not accumulate in the apex of the growing root hairs (Figure 5, B and D; Supplemental Figures S4, B and S7, B). For this reason, we analyzed all late endosomes carrying RabF2a-YFP within one homogeneous group. Characterization of movement distances of RabF2a-YFP compartments in bulging trichoblasts showed only negligible differences between control and *rhd2-1* (Figure 8, I and J). In addition, the maximum and average movement speed measurements provided similar values (Figure 8, K and L). Thus, the movement of late endosomes seems to be unaffected in *rhd2-1*.

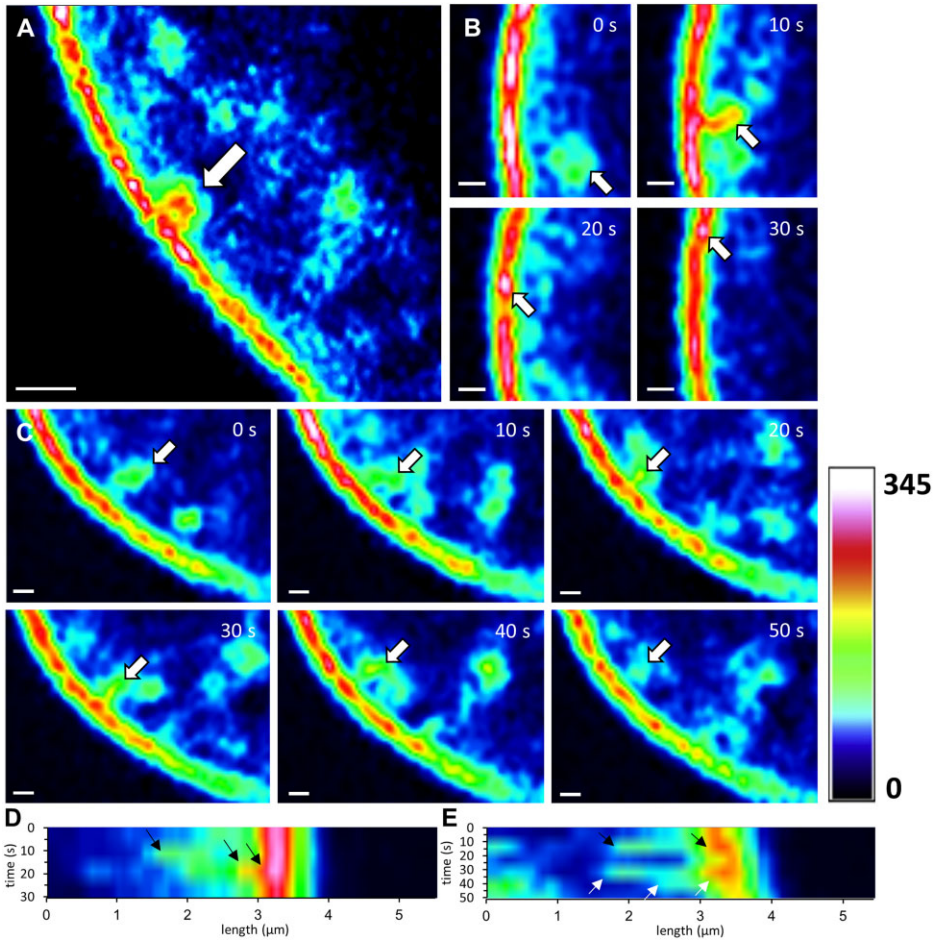

Figure 7 Time-course visualization of close contacts between moving compartments containing GFP-RHD2 and the apical PM in the root hair apex. A, Round-shaped compartment (arrow) in direct contact with strong GFP-RHD2 fluorescence signal in the apical PM. B and C, Two events of interactions between the compartments and the apical PM (Supplemental Movie S7) showing fast full integration with the PM (arrows; B, Supplemental Movie S8) or temporal contact lasting 50 s without full integration (fusion) with the PM (arrows; C, Supplemental Movie S9). The time-lapse imaging encompassed 30 s (B) and 50s (C). The fluorescence distribution is visualized through a semi-quantitative signal intensity using a pseudo-color-coded scale, where dark blue represents minimal intensity (0 arbitrary units) and white represents maximum intensity (345 arbitrary units). D and E, Kymographs showing interactions between the compartments and the apical PM either by full integration to the membrane (black arrows; D) or by approaching and a temporal contact with the PM (black arrows; E), but without fusion and followed by back movement to the cytoplasm (white arrows; E). Scale bar = 1 µm (A and B), 500 nm (C).

Distribution of GFP-RHD2 in root hairs after filipin III treatment

The delivery of compartments with GFP-RHD2 to the apical PM in bulges and growing root hairs requires physical interactions with the PM (Figure 7). Simultaneously, we identified and quantitatively characterized a sub-population of GFP-RHD2 compartments moving to and contacting the PM and subsequently moving back to the cytoplasm (Figures 6 and 7). Docking, eventual fusion, or recycling of these compartments back to the cytoplasm may require integral lipid membrane components. Structural sterols are integral components of plant membranes and are abundant in the apical PM of developing bulges and growing root hairs (Ovečka et al., 2010). In this study, we used filipin III, a vital probe for in vivo localization and sequestration of structural sterols (Grebe et al., 2003; Bonneau et al., 2010) in a physiologically high concentration that causes the formation of filipin–sterol complexes at the PM (Milhaud et al., 1988 ; Bonneau et al., 2010; Ovečka et al., 2010) and a rapid arrest of root hair tip growth (Jones et al., 2006; Ovečka et al., 2010). First, roots of the GFP-RHD2 line were treated with 10 µg.mL^{-1} filipin III using gentle perfusion directly at the microscope stage, and plants were examined by time-lapse live-cell imaging. Growing root hairs were photographed to visualize the cytoarchitecture using differential interference contrast (DIC) optics. At the same time, epifluorescence illumination allowed the monitoring of GFP-RHD2 localization and filipin III-induced PM staining during perfusion. The stabilized position of the sample at the microscope stage during the perfusion and sequential image acquisition (Figure 9) and monitoring of GFP-RHD2 accumulation at the tip by measuring fluorescence

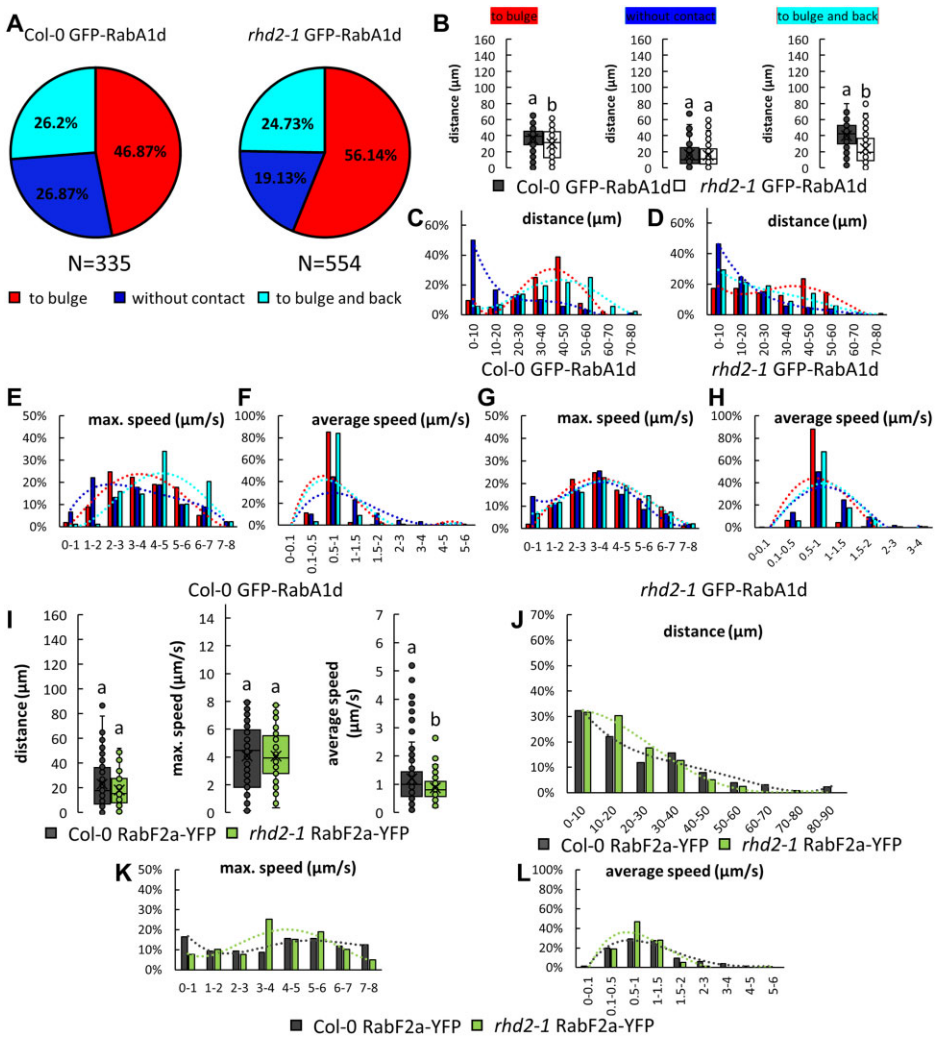

Figure 8 Qualitative and quantitative evaluation of endosomal compartments movements in developing bulges during root hair formation in Arabidopsis control and *rhd2-1* mutant lines. A, Quantitative determination of the ratio between the compartments showing targeted movement to the bulge (red), moving in the cytoplasm outside of the bulge (blue), and moving to the bulge and back (cyan) in the control line (Col-0) and *rhd2-1* mutant bearing early endosomal marker GFP-RabA1d. B, Quantitative evaluation of tracking distance for compartments containing GFP-RabA1d and moving either to the bulge (red), in the cytoplasm outside of the bulge (blue), or to the bulge and back (cyan) in Col-0 control line and *rhd2-1* mutant. C and D, Frequency distributions of distances for tracked compartments moving either to the bulge (red), in the cytoplasm outside of the bulge (blue), or to the bulge and back (cyan) in Col-0 control line (C) and *rhd2-1* mutant (D) bearing GFP-RabA1d marker. E–H, Frequency distributions of the maximum (E and G) and average speed (F and H) of the tracked compartments moving either to the bulge (red), in the cytoplasm outside of the bulge (blue), or to the bulge and back (cyan) in Col-0 control line (E and F) and *rhd2-1* mutant (G and H) carrying GFP-RabA1d. More than 335 compartments from two to four bulges from individual plants were analyzed. I, Quantitative evaluation of compartment tracking distances, their maximum, and average movement speed in bulges of Col-0 and *rhd2-1* mutant bearing late endosomal marker RabF2a-YFP. J–L, Frequency distributions of the distance (J), maximum speed (K), and average speed (L) of the analyzed compartments moving in bulges of Col-0 control line and *rhd2-1* mutant bearing RabF2a-YFP. More than 127 compartments from two to four bulges from individual plants were analyzed. Box plots show the first and third quartiles, split by the median (line) and mean (cross). Whiskers extend to include the maximum/minimum values. Different lowercase letters indicate statistical significance between treatments according to one-way ANOVA and subsequent LSD test ($P < 0.05$).

intensity profiles (Supplemental Figure S12) also provided the means for evaluation of the root hair tip growth. Root hairs before perfusion (time from 0 to 7 min) showed typical cytoarchitecture with tip-focused GFP-RHD2 localization (Figure 9, A and B). Analysis of the GFP fluorescence temporal distribution along a median profile in the form of a kymograph revealed continuous and sustained tip growth (Figure 9, C and D). To avoid any misinterpretations caused by changes induced by mechanical and osmotic disturbances during the application, perfusion with the control medium (mock treatment) was applied to control root hairs (Figure 9A). The control medium application induced a transient movement of the vacuole closer to the tip, slightly reducing the cytoplasm amount in the apical and subapical root hair zone (Figure 9A; DIC, time from

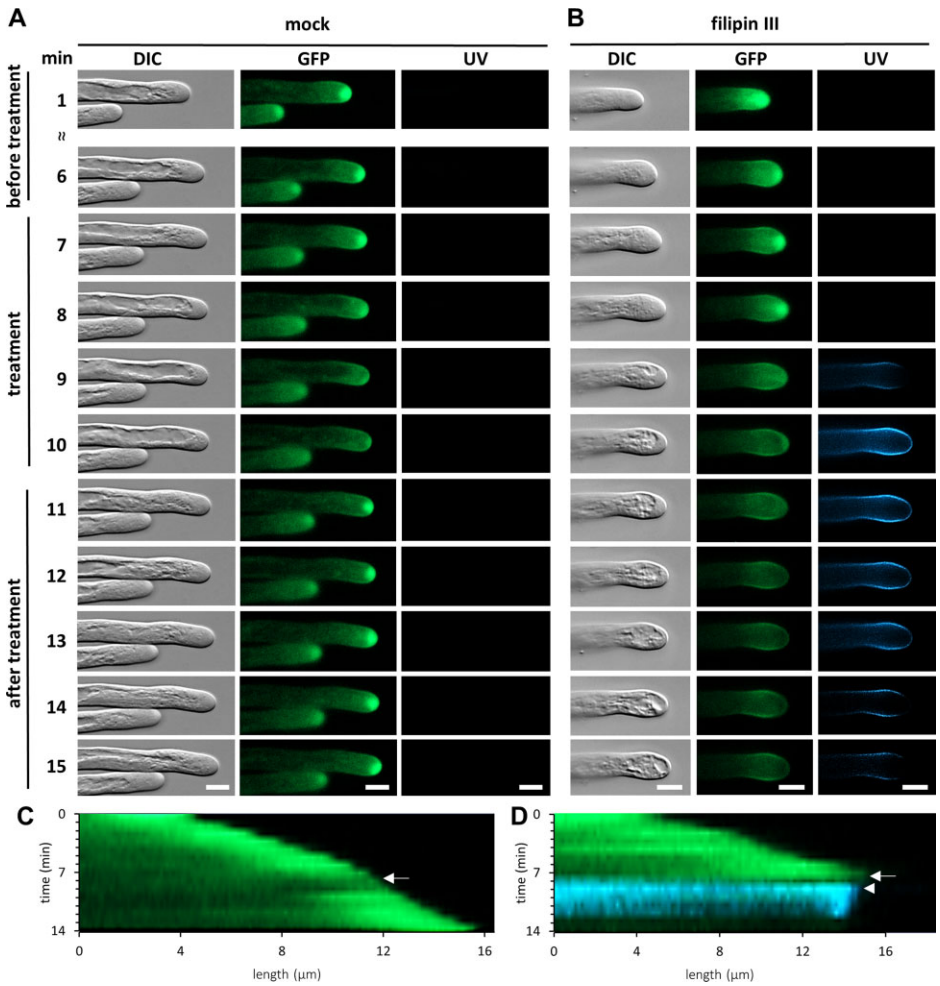

Figure 9 Inhibition of growing root hairs and changes of GFP-RHD2 localization after filipin III application. A and B, Growing root hairs imaged either by DIC for cytoarchitecture visualization, blue excitation fluorescence light for GFP-RHD2 localization (GFP), or ultra-violet excitation fluorescence light for visualization of PM staining by filipin III (UV). Root hairs show normal cytoarchitecture, tip-focused GFP-RHD2 localization, no signal in UV light (A and B), and sustained tip growth (C and D) before treatment (time from 0 to 7 min). During perfusion mock treatment (A), there was a transient reduction of the cytoplasm at the subapical root hair zone (A; DIC, 8–10 min; Supplemental Movie S10) and transient reduction of GFP-RHD2 in the apex (A; GFP, 9–10 min; Supplemental Movie S11; arrow in C), while it was reversibly restored and maintained up to the end of the experiments (up to 15 min; A and C). During perfusion filipin III treatment (B), root hairs stopped growth (arrow; D), their tips started to be invaded by round vacuoles (B; DIC, 9–10 min; Supplemental Movie S12), and GFP-RHD2 disappeared from the root hair apex (B; GFP, 9–10 min; Supplemental Movie S13). Simultaneously, filipin III-positive blue signal appeared at the PM (B; UV, 9–10 min; arrowhead in D). After a mock treatment (A), root hair cytoarchitecture (A; DIC, 11–15 min), tip-focused GFP-RHD2 localization (A; GFP, 11–15 min; Supplemental Figure S12), and root hair growth rate (C; 11–15 min) were regularly maintained and not disturbed. Root hair after filipin III treatment (B) showed disrupted cytoarchitecture such as vacuolated root hair apex (B; DIC, 11–15 min), lost GFP-RHD2 from the tip (B; GFP, 11–15 min; Supplemental Figure S12), filipin III-positive signal appeared at the PM (B; UV, 11–15 min), and completely blocked tip growth (D; 11–15 min). Acquisition of the GFP signal at 400 ms exposure time, and the filipin III signal at 200 ms exposure time was performed to gain optimal signal-to-noise ratio in GFP and UV channels (A and B). Reduction of filipin III-positive signal at the PM (B; UV, 11–15 min) was caused by bleaching induced by a wide-field epifluorescence illumination. Scale bar = 10 µm (A and B).

8 to 10 min). The reaction of root hairs to mock treatment was connected with a transient reduction of GFP-RHD2 fluorescence in the apex (Figure 9A; GFP, time from 8 to 10 min; arrow in Figure 9C). However, both parameters were reversibly restored to normal and maintained until the end of the experiments (Figure 9A; DIC, GFP, time up to 15 min). Thus, after a mock treatment, root hair cytoarchitecture (Figure 9A; DIC, from 11 to 15 min; Supplemental Movie S10), tip-focused GFP-RHD2 localization (Figure 9A; GFP, from 11 to 15 min; Supplemental Figure S12A; Supplemental Movie S11), and root hair tip growth rate (Figure 9C; from 11 to 15 min) were maintained and not considerably disturbed. As expected, epifluorescence ultra-violet illumination for filipin III excitation produced no signal upon mock treatment (Figure 9A; UV, time from 0 to 15 min).

Perfusion with filipin III caused the arrest of root hair tip growth (Figure 9B; DIC, time from 7 to 8 min) and was documented in the related kymograph (Figure 9D, arrow). Consequently, root hair tips were invaded by round

articulated vacuoles that irreversibly persisted until the end of the experiments (Figure 9B; DIC, time from 9 to 15 min). As the tip growth was arresting, GFP-RHD2 disappeared irreversibly from the root hair apex (Figure 9B; DIC, time from 9 to 15 min). Alongside the loss of GFP-RHD2, a filipin III-positive blue signal appeared at the PM (Figure 9B; UV, time from 9 to 15 min; arrowhead in Figure 9D). Therefore, root hairs after filipin III treatment showed disrupted cytoarchitecture due to massive vacuolation of the root hair apex (Figure 9B; DIC, from 9 to 15 min; Supplemental Movie S12), a loss of GFP-RHD2 from the tip (Figure 9B; GFP, from 9 to 15 min; Supplemental Figure S12B; Supplemental Movie S13), and accumulated filipin III-positive signal at the PM (Figure 9B; UV, from 9 to 15 min), resulting in blocked tip growth (Figure 9D; from 8 to 15 min).

Next, the root hairs of the GFP-RHD2 line were treated with 10 $\mu g.mL^{-1}$ filipin III for 10 min, and subcellular changes in GFP-RHD2 distribution were directly examined using a spinning disk microscope. The appearance of filipin III fluorescence in the PM of root hairs after application coincided with the tip growth arrest. Treatment with filipin III led to a layer-like accumulation of GFP-RHD2 closely associated with PM at the apex of root hairs (Figure 10, A and C). Because filipin III interacts specifically with sterols in the PM (Milhaud et al., 1988; Bonneau et al., 2010), filipin III-positive blue staining served as a PM marker under these circumstances. Therefore, the layer-like accumulation of GFP-RHD2 beneath the PM suggests that GFP-RHD2 was prevented from incorporating into the PM after filipin III treatment. Consistent with the localization pattern of GFP-RHD2 in the apical and subapical PM domains in control growing root hairs (Figures 2, J–M, 3, A and B, 4, A and E, 5, A and B, and 6, E and G; Supplemental Figure S1, C and E), the extent of layer-like accumulation of GFP-RHD2 after filipin III treatment reached only PM at the apical and subapical domains of root hairs (Figure 10A; Supplemental Figures S13B). This localization pattern was unique because equivalent experiments on GFP-RabA1d root hairs treated with filipin III revealed accumulation of early endosomal/TGN compartments in the apical part of the root hairs but not in close contact with filipin III-positive apical PM (Figure 10, B and E). Semi-quantitative analysis of the fluorescence intensity distribution using a profile function across the root hair apex (Figure 10C) revealed a "basal" level of GFP-RHD2 in filipin III-positive PM but mostly accumulated in a thin layer beneath the PM (Figure 10D). Simultaneously, the clear zone was depleted of GFP-RHD2 fluorescence after filipin III treatment (Figure 10, C and D). The same pattern of layer-like accumulation of GFP-RHD2 beneath the PM has been

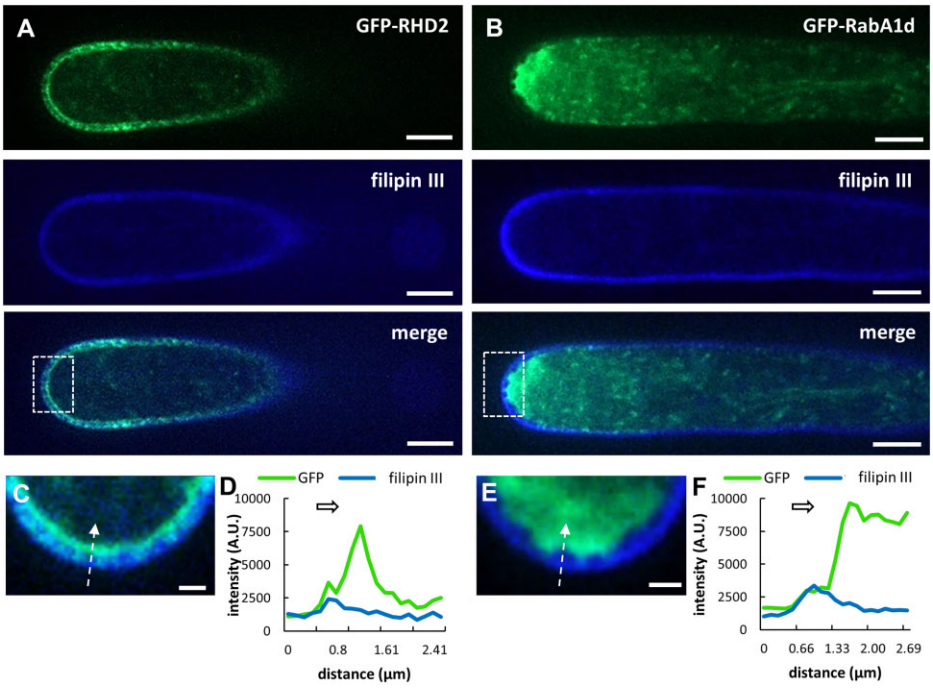

Figure 10 Localization analysis of GFP-RHD2 and GFP-RabA1d in root hairs after treatment with filipin III. A, Localization of GFP-RHD2 (green) in the root hair, filipin III-positive signal (blue) at the PM, and merged image showing the distribution pattern of GFP-RHD2 after filipin III treatment for 10 min. B, Localization of early endosomal marker GFP-RabA1d (green) in the root hair, filipin III-positive signal (blue) at the PM, and merged image showing the distribution pattern of GFP-RabA1d after filipin III treatment for 10 min. C, Detailed image of the apical part of the root hair within the white box in (A). Arrow indicates the position and the direction of the fluorescence intensity profile measurement. D, Fluorescence intensity profile of the GFP-RHD2 and filipin III-positive signal along the arrow in (C). The arrow above the curves indicates the direction of the measurement. E, Detailed image of the apical part of the root hair within the white box in (B). Arrow indicates the position and the direction of the fluorescence intensity profile measurement. F, Fluorescence intensity profile of the GFP-RabA1d and filipin III-positive signal along the arrow in (E). The arrow above the curves indicates the direction of the measurement. Scale bar = 5 µm (A and B), 1 µm (C and E).

observed in emerged bulges and elongated root hairs (Supplemental Figure S13). Interestingly, GFP-RabA1d accumulation in the clear zone after filipin III treatment showed a different pattern (Figure 10E) because it was detached and did not show direct contact with the filipin III-positive PM (Figure 10, E and F). Different GFP-RHD2 and GFP-RabA1d localization patterns after filipin III treatment were repeatedly observed in the apical part of treated root hairs (Supplemental Figure S14). In contrast, treatment of root hairs with filipin III did not cause any changes in the subcellular localization pattern of late endosomes visualized by RabF2a-YFP in root hairs (Supplemental Figure S15). Although root hair tip growth was arrested by filipin III treatment, the distribution of late endosomal compartments carrying RabF2a-YFP resembled the situation under control conditions (Supplemental Figure S4B). Moreover, similar results were obtained in the root hairs of the double GFP-RHD2 × mCherry-RabF2b transgenic line treated with filipin III (Supplemental Figure S16A). GFP-RHD2 accumulated strictly in close association with the apical PM, but late endosomal compartments carrying mCherry-RabF2b were distributed along the whole root hairs (Supplemental Figure S16A). Semi-quantitative fluorescence intensity evaluation at the root hair apex confirmed the close association of GFP-RHD2 with the apical PM and the absence of late endosomal compartments carrying mCherry-RabF2b in the clear zone (Supplemental Figure S16, B and C).

These data might indicate that the change in the GFP-RHD2 distribution pattern and related inhibition of the root hair tip growth by filipin III, reveal a specific role of structural sterols in the physical interaction of vesicular compartments containing GFP-RHD2 with the apical PM. To clarify this question, we performed an alternative treatment of growing root hairs with another independent inhibitor arresting root hair tip growth. We have used α-(2,4-dimethylphenylethyl-2-oxo)-IAA (auxinole), which is an auxin antagonist competing with auxin for binding sites on the auxin receptor TRANSPORT INHIBITOR RESPONSE 1 (TIR1), leading to the considerable reduction of root hair formation in *A. thaliana* (Smékalová et al., 2014). Root hairs after auxinole treatment rapidly arrested tip growth, which was not connected with considerable changes in the cytoarchitecture of root hair apex (Supplemental Figure S17). However, GFP-RHD2 gradually disappeared from the tip and the typical pattern of its distribution was lost. Only weak GFP-RHD2 signal remained at the PM (Supplemental Figure S17B). Detailed analysis confirmed the disappearance of GFP-RHD2 from the clear zone after auxinole treatment and revealed a localization of remaining GFP-RHD2 at the root hair periphery (Supplemental Figure S18, A–C). Staining of the PM with FM4–64 (Supplemental Figure S18D) confirmed the localization of remaining GFP-RHD2 in the PM, but not in a thin layer accumulated beneath the PM, typical for filipin III treatment. This was documented by both colocalization (Supplemental Figure S18E) and semi-quantitative analyses of the fluorescence intensity distribution using a profile function across the root hair apex (Supplemental Figure S18F).

These experiments with filipin III suggest that structural sterols, abundant in the apical PM of growing root hairs (Ovečka et al., 2010), might be involved in the dynamic relocation of GFP-RHD2. Upon filipin III treatment, we did not observe incorporation of GFP-RHD2 into the apical PM and have concluded that it might be caused by GFP-RHD2 inability to physically integrate into the apical PM. Based on the fact that PM labeling by filipin III leads to a concentration-dependent formation of filipin–sterol complexes at the ultrastructural level in plant cells (Grebe et al., 2003; Bonneau et al., 2010), including growing root hairs (Ovečka et al., 2010), this treatment leads irreversibly to arrest of the root hair tip growth (Ovečka et al., 2010). These results indicate the dependence of growing root hairs on RHD2/AtRBOHC integration to the apical PM, which might be mediated by structural sterols.

Discussion

The tip growth of root hairs is a highly polarized process depending on targeted vesicular transport, localized cell wall deposition, and PM extension at the growing tip. It is supported by tip-localized transmembrane gradients (Ca^{2+}, ROS, and pH) and by polarized organization and dynamics of the cytoskeleton (Šamaj et al., 2006). The establishment and maintenance of these gradients in root hairs are orchestrated by the NADPH oxidase AtRBOHC/RHD2 (Foreman et al., 2003) activated by Rop GTPases (Jones et al., 2007) accumulated at the site of future root hair initiation (Molendijk et al., 2001; Jones et al., 2002). Loss of AtRBOHC/RHD2 function in *rhd2* mutants leads to the interruption of root hair tip growth. Nevertheless, fully rescued root hair development has been achieved by transforming *rhd2* by GFP-tagged AtRBOHC/RHD2 under the control of the native promoter (Takeda et al., 2008). Cell type-specific and developmentally regulated localization of GFP-RHD2 in trichoblasts revealed its selective accumulation in bulges and tips of developing root hairs (Takeda et al., 2008). Using different advanced microscopy methods, we qualitatively and quantitatively characterized the subcellular localization of GFP-RHD2. We visualized dynamic vesicular compartments linked with the formation and maintenance of the apical PM domain during root hair development. In root development, these compartments appeared first in the epidermis of the root hair formation zone (the proximal part of the root elongation zone and in the differentiation zone). The number of compartments was substantially higher in the trichoblasts. This localization pattern, spatiotemporally related to root hair formation, is consistent with quantitative microarray analysis of roots, showing enhanced *RHD2* transcription in differentiation and elongation root zones, epidermal cells, and root hairs (Chapman et al., 2019). Next, we used a quantitative particle tracking approach to characterize the temporal and spatial GFP-RHD2 subcellular redistribution pattern during root hair initiation and growth. This analysis

revealed a mode of targeted GFP-RHD2 delivery to the apical PM domain of developing bulges and growing root hairs. Notably, the PM area containing GFP-RHD2 was restricted, and the range of this area corresponded with particular stages of root hair development.

Localized delivery of GFP-RHD2 and its incorporation into the PM by motile compartments raises questions about their molecular signatures. As expected, the membrane-specific dye FM4–64 colocalized with GFP-RHD2 at the PM of root hairs in the apical and subapical zones where GFP-RHD2 was restricted. In addition, labeling of growing root hairs with FM4–64 revealed a high degree of colocalization with GFP-RHD2 in compartments moving in the cytoplasm of root hairs. This unequivocally indicated their vesicular nature. The short incubation time of growing root hairs with FM4–64 serves to visualize early endocytic compartments (Ovečka et al., 2005). Colocalization studies with early endosomes/TGN (GFP-RabA1d; Ovečka et al., 2010; Berson et al., 2014) or late endosomes (RabF2a-YFP; Voigt et al., 2005; Berson et al., 2014) confirmed that a short FM4–64 application is suitable for the localization of early but not late endosomes. To corroborate these data, we analyzed colocalization in double transgenic lines carrying GFP-RHD2 together with mCherry-VTI12 (an early endosomal/TGN marker; Geldner et al., 2009) and mCherry-RabF2b (a late endosomal marker; Geldner et al., 2009). Using this approach, the colocalization of GFP-RHD2 with the early endosomal/TGN marker mCherry-VTI12 was confirmed in the cytoplasmic compartments of growing root hairs. The maximum speed of motile compartments containing GFP-RHD2 in root hairs was typically 4–8 $\mu m\ s^{-1}$. This is consistent with the dynamic properties of early endosomal compartments carrying molecular markers GFP-RabA1d and YFP-VTI12, with a maximal speed of 6–9 $\mu m\ s^{-1}$ (von Wangenheim et al., 2016).

Notably, the spatial control of GFP-RHD2 incorporation into the apical PM was closely related to the nonuniform pattern of vesicular movements. The ratio of the compartments moving and fusing with the apical PM, those moving toward, contacting the PM, and subsequently moving back to the cytoplasm, or those moving in the cytoplasm without any contact with the apical PM, changed with different stages of root hair development. The particle tracking analysis provided quantitative parameters of these movements and their specific features, especially in compartments coming into contact with the PM. The enlargement of the bulging domain was tightly connected with the higher portion of compartments moving to the apical PM and fusing with it. This corresponded with the gradual enlargement of the apical PM area, incorporating and accumulating GFP-RHD2. In contrast, there was an increase in the fraction of compartments contacting the PM and subsequently moving back to the cytoplasm during the growth of root hairs. This likely represents the active recycling of GFP-RHD2 between the PM and motile vesicular compartments in the cytoplasm. These data also indicate that compartments containing GFP-RHD2 are spatiotemporally specialized in particular stages of root hair formation. Consequently, the ratio between different compartment types responsible for the rate of GFP-RHD2 incorporation into the PM and/or recycling was regulated according to the developmental stage of the root hair.

We also tested a possible link between AtRBOHC/RHD2 and the movement of endosomal compartments through detailed quantitative characterization of early endosomes/TGN and late endosomes in the *rhd2-1* mutant. We compared early endosomal/TGN compartments visualized by GFP-RabA1d in the control line, specifically those moving to the bulge or those moving to the bulge and back to the trichoblast, and found differences in their speed and trajectory values. The same comparison in the *rhd2-1* mutant carrying GFP-RabA1d, however, revealed no differences. It seems that the loss of function of AtRBOHC/RHD2 in the *rhd2-1* mutant influenced, at least partially, the dynamic behavior of early endosomes/TGN in bulges. Comparison with late endosomes visualized by RabF2a-YFP under the same circumstances revealed no differences between the control and *rhd2-1* mutant. These results indicate that *AtRBOHC/RHD2* loss-of-function mutation affects only early endosomal/TGN compartments, verifying the crucial role of early endosomal/TGN compartments in root hair formation and growth. Overall, live-cell localization during root hair initiation and growth by advanced microscopy indicated the involvement of GFP-RHD2 in the specialization and maintenance of apical PM domains in bulges and tip-growing root hairs and targeted delivery to the cortical cytoplasm and the clear zone in dynamic vesicular compartments.

Finally, we tested the possible role of structural sterols in docking and fusion of compartments containing GFP-RHD2 with the apical PM of growing root hairs. The subcellular localization of structural sterols can be performed using vital fluorescent probes. Filipin III is a polyene antibiotic fluorochrome suitable for the localization of structural sterols in animal (Nichols et al., 2001), yeast (Wachtler et al., 2003), and plant cells (Grebe et al., 2003; Boutté et al., 2009; Liu et al., 2009; Bonneau et al., 2010). Specific accumulation of filipin III signal was observed in the PM of the prebulging site, developing bulges, and at the tips of growing root hairs (Ovečka et al., 2010). At higher concentrations or after prolonged exposure, filipin III induced the formation of filipin–sterol complexes (Milhaud et al., 1988; Bonneau et al., 2010; Ovečka et al., 2010). This leads to PM damage and changes in physiological functions, and such treatments block root hair tip growth and affect vesicular trafficking (Ovečka et al., 2010). Treatment of root hairs with filipin III allowed us to visualize sterols in the PM of growing root hairs (Figure 9), which was inevitably connected with the arrest of tip growth. Detailed microscopic analysis revealed that filipin III might prevent the correct incorporation of GFP-RHD2 into the apical PM zone (Figure 10). Ultrastructural examination documented that concentrations of filipin III at and $> 10\ \mu g.mL^{-1}$ cause the formation of filipin–sterol complexes at the PM (Grebe et al., 2003; Bonneau et al., 2010;

Ovečka et al., 2010). The appearance of filipin–sterol complexes at the PM was immediately connected with PM rigidification. It triggered ion leakage, extracellular pH alkalization, and changes in signaling dependent on protein kinase-mediated phosphorylation (Bonneau et al., 2010). Thus, the formation of filipin III-induced complexes with sterols most likely inhibits sterol functions at the PM, possibly including the proper incorporation of GFP-RHD2 to the apical PM zone of growing root hairs. It was reported previously that treatment with the sterol-disrupting agent methyl-β-cyclodextrin caused redistribution, clustering, and changes in the diffusion properties of GFP-RBOHD, a fluorescently tagged NADPH oxidase involved in plant defense within the PM of the hypocotyl epidermal cells (Hao et al., 2014). Defective localization of RHD2 NADPH oxidase in root hairs was observed in a sterol-deficient *drought hypersensitive/squalene epoxidase 1-5* mutant of *A. thaliana* (Posé et al., 2009; Sena et al., 2017). The link between structural sterols at the PM and root hair formation might be mediated by a regulatory role of Rho of plants (ROPs) such as ROP2, ROP4, and ROP6. ROPs are recruited at the site of future root hair initiation by RopGEF3 (Denninger et al., 2019) and accumulate in bulges and the apex of growing root hairs (Molendijk et al., 2001; Jones et al., 2002). ROP2 and ROP4 activate AtRBOHC/RHD2 for localized ROS production during root hair formation (Carol et al., 2005). ROPs activation leads to transient S-acylation, which is required for their functionality and stabilizes their interaction with the PM and accumulation in lipid rafts (Sorek et al., 2011, 2017). ROP2 and ROP6 colocalize with sterol-enriched PM domains at root hair formation sites and the tips of growing root hairs (Stanislas et al., 2015).

Surprisingly, unlike GFP-RabA1d, GFP-RHD2 in filipin III-treated root hairs accumulated within a thin layer closely associated with the inner cytoplasmic side of the apical PM, and the GFP-RHD2 signal was depleted in the clear zone. Independent treatment with auxinole, arresting similarly root hair tip growth, led to a different GFP-RHD2 distribution pattern, suggesting a specific role of structural sterols, targeted by filipin III. These data indicate that structural sterols, which are responsible for membrane fluidity and the formation of lipid nanodomains, might participate in the correct insertion of GFP-RHD2 to the apical PM in root hairs. Such layer-like accumulation of GFP-RHD2 beneath the apical PM might suggest that the physical incorporation is prevented, and the depletion of GFP-RHD2 compartments from the clear zone might indicate that recycling from the PM was inhibited. Although the complete functionality of the model includes the endogenous RHD2, which is still present and functionally relevant in the examined transgenic line, this observation indicates that structural sterols might be involved in localized anchoring and maintenance of GFP-RHD2 in the apical PM zone of developing root hairs.

Materials and methods

Plant material preparation

Experiments were performed with plants of Arabidopsis (*A. thaliana*), wild-type of the Col-0 ecotype, *rhd2-1* (Foreman et al., 2003) mutant, and stably transformed *A. thaliana* plants (of Col-0 wild-type background) carrying constructs with GFP-RHD2 (Takeda et al., 2008) and fluorescent markers of endosomal compartments. Stable transgenic lines in the Col-0 background, bearing fluorescent markers of endosomal compartments, were prepared by crossing. Plants of the *rhd2-1* mutant, used as female donors, were crossed with transgenic plants bearing fluorescent markers for early endosomes/TGN, GFP-RabA1d (Ovečka et al., 2010), or late endosomes, RabF2a-YFP (Voigt et al., 2005). Transgenic plants bearing fluorescent markers of endosomal compartments were used as male donors. Transgenic plants with N-terminal fusion of RHD2 with GFP under the control of the *RHD2* promoter (GFP-RHD2 line in the Col-0 background; Takeda et al., 2008), were crossed with transgenic plants carrying fluorescent markers of endosomal compartments (Wave line W13R producing mCherry-VTI12 for early endosomes/TGN; Geldner et al., 2009, and Wave line W2R producing mCherry-RabF2b for late endosomes; Geldner et al., 2009). Transgenic plants with GFP-RHD2 were used as female donors in crossings. The progeny of the F1 generation was selected according to fluorescence signals using an Axio Zoom.V16 fluorescence stereomicroscope (Carl Zeiss, Germany), and plants of the F2 or F3 generations were used for experiments. We analyzed the transmission of the *GFP-RHD2* and red marker alleles in the F2 and F3 generations by phenotypical analysis. As expected, the progeny of heterozygous plants consisted of ∼50% of the individuals simultaneously carrying GFP and red fluorescence. GFP fluorescence alone was detected in ∼25% of plants, analogous to mCherry (Table 1). Lines showing both types of fluorescence with the wild-type root hair phenotype were used further for the colocalization studies.

In vitro cultivation

Seeds of *A. thaliana* control, mutant, and transgenic lines were surface-sterilized and planted on 1/2 Murashige and Skoog (MS) medium (Murashige and

Table 1 F2 progeny after the crossing of the transgenic lines bearing GFP-tagged RHD2 with mCherry-tagged endosomal markers

Crossed Lines	Phenotype (Fluorescence)				No. of Plants
	GFP + mCherry (%)	GFP (%)	MCherry (%)	None (%)	
GFP-RHD2 × *mCherry-RabF2b*	49	25	21	5	118
GFP-RHD2 × *mCherry-VTI12*	55	21	17	7	94

Skoog, 1962) without vitamins, solidified with 0.6% (w/v) Gellan gum (Alfa Aesar, Thermo Fisher Scientific, Heysham, UK). Petri dishes with seeds were stratified at 4°C for 3 d for synchronized germination. After stratification, seeds were cultivated vertically in an environmental chamber at 21°C, 70% humidity, and 16-h/8-h light/dark cycle. The illumination intensity was 130 μmol $m^{-2}s^{-1}$.

LSFM

Samples for LSFM were prepared as described by Ovečka et al. (2015). Seeds of GFP-RHD2 line were surface sterilized and transferred to round 90 × 25 mm Petri dishes filled with 80 mL of modified MS medium (Ovečka et al. 2014) at pH 5.7, solidified with 0.5% (w/v) Gellan gum. After germination, the roots began to grow into the medium gravitropically. Three-day-old plants were inserted into the fluorinated ethylene propylene (FEP) tubes with the medium surrounding the root (root was embedded in the medium, and the upper green part was exposed to air). The samples were transferred to a pretempered (22°C) observation chamber of the LSFM filled with a modified liquid MS medium. The agar block with the plant was partially pushed out from the FEP tube into the liquid medium for imaging of the root tip not surrounded by FEP tube walls. After 30 min of stabilization, plants were observed using a light-sheet Z.1 fluorescence microscope (Carl Zeiss, Germany) equipped with two LSFM 10×/0.2 NA illumination objectives (Carl Zeiss, Germany), Plan-Apochromat 20×/1.0 NA water immersion detection objective (Carl Zeiss, Germany), and the PCO Edge sCMOS camera (PCO AG, Germany) with an exposure time of 40 ms. Each individual plant represented an independent biological replicate, and >8 plants were analyzed. Imaging was carried out using dual-side illumination and pivot scan mode with a light-sheet thickness of 4.52 μm. GFP was excited at 488 nm using 2% of relative laser power level, and detected between 505 and 545 nm with BP505–545 emission filter. Images were acquired in three subsequent views aligned to each other in the root growth direction (along the *y* coordinate) at time points of every 5 min in *Z*-stack mode for 15 h. Image scaling in *x*, *y*, and *z* was adjusted to 0.228 × 0.228 × 0.477 μm, encompassing the volume of 438.69 × 438.69 × 229.79 μm (*x* × *y* × *z*).

Airyscan CLSM and spinning disk (SD) microscopy

Plants 2- to 3-day-old were transferred to microscopy chambers containing liquid modified MS medium according to Ovečka et al. (2005, 2014). After manipulation with plants during sample preparation, the subsequent stabilization period for 24 h allowed undisturbed growth of the root and the formation of new root hairs. The development of root hairs in more than 10 individual plants was observed using a confocal laser scanning microscope LSM880 equipped with Airyscan (Carl Zeiss, Germany) and a Cell Observer SD Axio Observer Z1 spinning disk microscope (Carl Zeiss, Germany). Airyscan CLSM was used for qualitative and quantitative characterization of GFP-RHD2-positive compartments during root hair development and growth. Image acquisition was performed with a 20×/0.8 NA dry Plan-Apochromat objective (Carl Zeiss, Germany). The samples were imaged with an excitation laser line of 488 nm and BP420–480 + BP495–550 emission filters for GFP detection. The laser power did not exceed 0.8% of the available laser intensity range. The samples were scanned every 706 ms with 700 ms of exposure time using a 32 GaAsP detector. Pixel dwell time was set up to 1.98 μs, and with default settings of the gain level the image scaling was set up to 0.074 × 0.074 × 0.397 μm (*x* × *y* × *z*). A spinning disk microscope equipped with alpha Plan-Apochromat 100×/1.57 NA DIC Korr oil immersion objective (Carl Zeiss, Germany) was used for colocalization analyses. The samples were imaged using an excitation laser line of 405 nm and emission filter BP450/50 for filipin III signal detection, excitation laser line of 488 nm and emission filter BP525/50 for GFP signal detection, excitation laser line of 514 nm, and emission filter BP535/30 for YFP signal detection, excitation laser line of 514 nm and emission filter BP690/50 for FM4-64 signal detection, and excitation laser line of 561 nm and emission filter BP629/62 for the mCherry signal detection. The excitation laser power level for all lasers used was set up to 50%, and the image scaling for all channels was 0.133 × 0.133 μm in *x* × *y* dimensions, and with the *z* dimension 0.52 μm for the filipin III channel, 0.63 μm for the GFP channel, 0.66 μm for the YFP channel, 0.75 μm for the mCherry channel, and 0.92 μm for the FM4–64 channel. Images were acquired sequentially or simultaneously with two Evolve 512 EMCCD cameras (Photometrics) with an exposure time of 700 ms. The samples were scanned every 731 ms using a camera-streaming mode.

FM4–64 staining, filipin III, and auxinole application

FM4–64 (Thermo Fisher Scientific, Waltham, MA, USA) was used as the PM and vesicular marker in the root hairs. Filipin III (Sigma-Aldrich, St Louis, MO, USA) was used as a vital probe for PM structural sterols, allowing the formation of filipin–sterol complexes in root hairs at higher concentrations. Auxinole (MedChemExpress, Monmouth Junction, NJ, USA), a potent auxin antagonist, was used for arresting root hair tip growth. In five independent plants per treatment, FM4–64 (4 μmol.L^{-1}), filipin III (10 μg.mL^{-1}), and auxinole (20 μmol.L^{-1}) in modified liquid MS medium were individually applied by perfusion directly to the microscopy chamber. The total volume of the modified liquid MS medium with FM4–64, filipin III, or auxinole applied was 100 μL, added in 10 separate steps of 10 μL each for 10 min. After perfusion, the plants were directly observed using a spinning disk microscope.

Life imaging of GFP-RHD2 in root hairs after filipin III and auxinole application

Plants 2- to 3-day-old were transferred to microscopy chambers containing liquid modified MS medium according to Ovečka et al. (2005, 2014). Subsequent stabilization for 24 h in a glass cuvette in an environmental chamber allowed the continuation of root growth and the formation of new root

hairs. Growing root hairs (n = 3–5 root hairs from five plants) were observed using an epifluorescence microscope Zeiss Axio Imager M2 equipped with DIC optics and epifluorescence metal halide source illuminator HXP 120 V (Zeiss, Oberkochen, Germany), and analyzed using Zeiss ZEN 2012 Blue software (Zeiss, Germany). Root hairs were recorded at 1 min intervals for 5 min before the application, then for another 5 min throughout the application of mock, 10 $\mu g.mL^{-1}$ filipin III, or 20 $\mu mol.L^{-1}$ auxinole in modified liquid MS medium, respectively, and 5 min after application. Modified MS medium without inhibitors was used as a mock treatment. The total volume of applied solutions (control medium, filipin III, and auxinole) was 50 µL, added sequentially in five separate steps of 10 µL each. Gentle application by perfusion was performed directly at the microscope stage in the sample chambers at the respective time points of acquisition. Imaging was performed with a Plan-Neofluar 40 × /0.75 NA dry objective and documented with a Zeiss AxioCam ICm1 camera. A filter set providing a wavelength of 450–490 nm for the excitation and 515–565 nm for the emission at 400-ms exposure time was used to visualize the GFP signal. For the filipin III signal, the filter set provided an excitation wavelength of 335–383 nm and an emission wavelength of 420–470 nm was used. The exposure time was 200 ms for both filipin III and DIC channel acquisitions. The image scaling for both channels was 0.116 × 0.116 µm in $x \times y$ dimensions, and with the z dimension 1.65 µm for the filipin III channel, and 1.81 µm for the GFP channel.

Colocalization analysis

The colocalization of fluorescence signals was analyzed using a spinning disk microscope by simultaneous signal acquisition with two independent Evolve 512 EMCCD cameras. After camera calibration for proper alignment, the fluorescence signals of the two markers were imaged and recorded using a camera streaming mode. Semi-quantitative signal intensity analysis was performed on one selected Z-stack of the scanned area. The signal intensity and mode of colocalization were analyzed in double transgenic lines GFP-RHD2 × mCherry-VTI12 and GFP-RHD2 × mCherry-RabF2b. Similarly, the fluorescence intensity was determined in single transgenic lines GFP-RHD2, GFP-RabA1d, and RabF2a-YFP stained with FM4–64. Profiles for quantitative signal intensity distribution and colocalization were generated using Zen Blue 2014 software (Carl Zeiss, Germany) and graphically edited in Microsoft Excel. Quantitative colocalization analysis of vesicular compartments was conducted within selected ROIs from five individual root hairs at five different time points. Three ROIs selected at each analyzed time point led to 75 measurements of vesicular compartments performed in total. Analogously, colocalization analysis was performed on PMs from five individual root hairs at five different time points. A particular ROI covering the membrane area of each respective time point was selected, providing 25 measurements on PMs in total. Selected ROIs of vesicles and membranes of double lines (GFP-RHD2 × mCherry-VTI12 and GFP-RHD2 × mCherry-RabF2b) and FM4–64 staining of GFP-RHD2, GFP-RabA1d, and RabF2a-YFP lines were subjected to quantitative colocalization analysis using Pearson's correlation coefficients according to Costes et al. (2004) in Zen Blue 2014 software (Carl Zeiss, Germany). The results were graphically edited using Microsoft Excel.

3D rendering of GFP-RHD2 distribution

Data obtained by LSFM time-lapse imaging from growing primary roots and root hairs of the GFP-RHD2 line were subjected to 3D rendering. In Zen 2014 software, black edition (Carl Zeiss, Germany), a subset of selected time-points (lasting for 4 h and 25 min of imaging) was created from the whole volume of the root (containing 483 Z-stacks). The subsets were selected to capture the different developmental stages of root hair formation in the root differentiation zone. The output data were imported into Arivis Vision4D version 2.12.6 software (Arivis AG, Rostock, Germany) and automatically converted to the *.sis file. Subsequently, data were visualized as 3D objects by activating the 4D viewer in the Viewer Types Panel. 3D objects were rendered in the maximum intensity mode. The color scale was switched to rainbow coloring to enhance the contrast visibility of the fluorescence signal intensities and distribution. The lowest and highest saturation points were adjusted to 219 (black) and 427 (red), respectively. For 3D visualizations of primary root cross-sections, clipping around a region of interest was adjusted using a 4D clipping panel and ROI tab. Videos were configured by arranging keyframes and rendered as movies for export in the storyboard extension. Animations were prepared by clipping the 3D model against the y- and z-planes in a 4D clipping panel and using rotation and zoom tools.

Single-particle tracking of compartments containing GFP-RHD2

Arivis Vision4D program, version 3.1.4. (Arivis AG, Germany) was used for quantitative tracking of the GFP-RHD2 compartments. Three-day-old plants were imaged using Airyscan CLSM. Different stages of root hair development were selected, and one particular Z-stack of the field of view was imaged for 60 s. Acquired data were processed and quantified using the Tracked cells function of the Arivis software. Before analysis, the following conditions were set up for normalization: (1) the highest and lowest fluorescence intensity thresholds were set to 30 and 410, respectively; (2) the distance of compartment movement recorded during one time period should not exceed 5 µm; (3) accepted compartments did not disappear from the image plane for more than two time periods during acquisition; and (4) the accepted compartment surface area was always in the range of 0.5–3 μm^2. Characterized parameters were minimum, maximum, and average speed, the distance of GFP-RHD2 compartments moving in different stages of root hair development, namely in the early bulges, late bulges, short growing root hairs, and longer growing root hairs. The analyzed compartments were

divided into the following subgroups: moving to and contacting the apical PM, moving in the cytoplasm without any contact with the PM, and contacting the PM and moving back to the cytoplasm. A comparison was made between compartments moving outside the bulging domain in trichoblasts and those moving in atrichoblasts. The individual color-coded trajectories of the analyzed compartments were displayed directly in the images. Arivis software was also used to generate the 2.5D fluorescence intensity profiles.

Data analysis and graphical presentation

Kymographs were generated from time-lapsed images acquired by LSFM, Airyscan CLSM, and SD using the appropriate plugin of Zen software (Blue version). All graphs were prepared using Microsoft Excel software. Statistical significance ($P < 0.05$) was determined using the STATISTICA 12 (StatSoft, TIBCO Software Inc., Palo Alto, CA, USA) by analysis of variance (ANOVA) and subsequent Fisher's least significant difference (LSD) tests ($P < 0.05$).

Accession numbers

Sequence data from this article can be found in the GenBank/EMBL/TAIR (https://www.arabidopsis.org) data libraries under accession numbers: AT5G51060 (*RHD2*), AT4G18800 (*RABA1D*), AT1G26670 (*VTI12*), AT5G45130 (*RABF2A*), and AT3G62980 (*TIR1*).

Supplemental data

The following materials are available in the online version of this article.

Supplemental Figure S1. Semi-quantitative analysis of root hair tip growth rate in individual developmental stages.

Supplemental Figure S2. Semi-quantitative analysis of the tip-focused GFP-RHD2 spatial signal intensity distribution obtained using the 2.5D rendering function in different stages of root hair development.

Supplemental Figure S3. Example of a quantitative colocalization analysis between FM4–64 and GFP-RHD2.

Supplemental Figure S4. Colocalization analysis of early and late endosomal markers with selective membrane styryl dye FM4–64 in growing root hairs.

Supplemental Figure S5. Example of a quantitative colocalization analysis between FM4–64 and early endosomal marker GFP-RabA1d.

Supplemental Figure S6. Example of a quantitative colocalization analysis between FM4–64 and late endosomal marker RabF2a-YFP.

Supplemental Figure S7. Localization of early and late endosomal markers in growing root hairs of control lines.

Supplemental Figure S8. Example of a quantitative colocalization analysis between GFP-RHD2 and early endosomal/TGN marker mCherry-VTI12.

Supplemental Figure S9. Example of a semi-quantitative colocalization analysis between GFP-RHD2 and late endosomal marker mCherry-RabF2b.

Supplemental Figure S10. Quantitative evaluation of the tracking parameters of compartments containing GFP-RHD2 in different stages of root hair development.

Supplemental Figure S11. Qualitative determination and quantitative tracking of moving compartments containing GFP-RHD2 in atrichoblasts and trichoblasts outside of the bulging zone.

Supplemental Figure S12. Changes of GFP-RHD2 localization in growing root hairs after filipin III application.

Supplemental Figure S13. Localization analysis of GFP-RHD2 in bulge and root hair after treatment with filipin III.

Supplemental Figure S14. Localization analysis of GFP-RHD2 and GFP-RabA1d in root hairs after treatment with filipin III.

Supplemental Figure S15. Localization analysis of RabF2a-YFP in root hairs after treatment with filipin III.

Supplemental Figure S16. Localization analysis of GFP-RHD2 and mCherry-RabF2b in root hairs after treatment with filipin III.

Supplemental Figure S17. Inhibition of growing root hairs and changes of GFP-RHD2 localization after auxinole application.

Supplemental Figure S18. Localization analysis of GFP-RHD2 in root hairs treated by auxinole.

Supplemental Movie S1. 3D maximum intensity projection and a volumetric rendering of a pseudo-color-coded semi-quantitative fluorescence intensity distribution of GFP-RHD2 in the root hair formation zone in Arabidopsis from LSFM imaging.

Supplemental Movie S2. Time-lapse imaging of developing root hair in the root of transgenic Arabidopsis plant carrying GFP-RHD2 using LSFM. Exposure time 40 ms, time point every 5 min, imaging time 220 min.

Supplemental Movie S3. Time-lapse imaging of developing late bulge using Airyscan CLSM showing polarized accumulation of GFP-RHD2 at the apical PM domain and cortical cytoplasm in a pseudo-color-coded semi-quantitative fluorescence intensity distribution. Exposure time 700 ms, time point every 9.8 s, imaging time 16 min.

Supplemental Movie S4. Time-lapse imaging of short growing root hair using Airyscan CLSM showing polarized accumulation of GFP-RHD2 at the apical PM domain and cortical cytoplasm in a pseudo-color-coded semi-quantitative fluorescence intensity distribution. Exposure time 700 ms, time point every 9.8 s, imaging time 8 min.

Supplemental Movie S5. Time-lapse imaging of long growing root hair using Airyscan CLSM showing polarized accumulation of GFP-RHD2 at the apical PM domain and cortical cytoplasm in a pseudo-color-coded semi-quantitative fluorescence intensity distribution. Exposure time 700 ms, time point every 9.8 s, imaging time 8 min.

Supplemental Movie S6. Time-lapse imaging of non-growing root hair using Airyscan CLSM showing polarized accumulation of GFP-RHD2 at the apical PM domain and cortical cytoplasm in a pseudo-color-coded semi-quantitative fluorescence intensity distribution.

Exposure time 700 ms, time point every 9.8 s, imaging time 3 min.

Supplemental Movie S7. Time-lapse imaging of close contacts (arrows) between moving compartments containing GFP-RHD2 and the apical PM in the apex of late bulge using Airyscan CLSM in a pseudo-color-coded semi-quantitative fluorescence intensity distribution. Exposure time 700 ms, time point every 9.8 s, imaging time 60 s, maximum intensity projections of two Z-stacks.

Supplemental Movie S8. Time-lapse imaging of contact between moving compartment containing GFP-RHD2 and the apical PM in the apex of a late bulge showing fast full integration. Imaging using Airyscan CLSM in a pseudo-color-coded semi-quantitative fluorescence intensity distribution. Exposure time 700 ms, time point every 9.8 s, imaging time 30 s, maximum intensity projections of two Z-stacks.

Supplemental Movie S9. Time-lapse imaging of contact between moving compartment containing GFP-RHD2 and the apical PM in the apex of a late bulge showing temporal contact without full integration. Imaging using Airyscan CLSM in a pseudo-color-coded semi-quantitative fluorescence intensity distribution. Exposure time 700 ms, time point every 9.8 s, imaging time 50 s, maximum intensity projections of two Z-stacks.

Supplemental Movie S10. Time-lapse imaging of growing root hair using DIC optics showing growth rate and cytoarchitecture during perfusion application of control medium. Exposure time 200 ms, time point every 1 min, imaging time 14 min.

Supplemental Movie S11. Time-lapse imaging of growing root hair using fluorescence excitation for localization of GFP-RHD2 during perfusion application of control medium. Exposure time 400 ms, time point every 1 min, imaging time 14 min.

Supplemental Movie S12. Time-lapse imaging of growing root hair using DIC optics showing growth rate and cytoarchitecture during perfusion application of filipin III. Exposure time 200 ms, time point every 1 min, imaging time 14 min.

Supplemental Movie S13. Time-lapse imaging of growing root hair using fluorescence excitation for localization of GFP-RHD2 during perfusion application of filipin III. Exposure time 400 ms, time point every 1 min, imaging time 14 min.

Acknowledgments

We thank Liam Dolan for the seeds of the *rhd2-1* mutant and the GFP-RHD2 line. We would like to thank Editage (www.editage.com) for English language editing.

Funding

This work was supported by the Czech Science Foundation GAČR (project Nr. 19-18675S) and by the ERDF project "Plants as a tool for sustainable global development" (No. CZ.02.1.01/0.0/0.0/16_019/0000827).

Conflict of interest statement: Authors declare that they have no conflicts of interests.

References

Berson T, Wangenheim D, Takáč T, Šamajová O, Rosero A, Ovečka M, Komis G, Stelzer EH, Šamaj J (2014) Trans-Golgi network localized small GTPase RabA1d is involved in cell plate formation and oscillatory root hair growth. BMC Plant Biol **14**: 252

Bonneau L, Gerbeau-Pissot P, Thomas D, Der C, Lherminier J, Bourque S, Roche Y, Simon-Plas F (2010) Plasma membrane sterol complexation, generated by filipin, triggers signalling responses in tobacco cells. Biochim Biophys Acta **1798**: 2150–2159

Bottanelli F, Foresti O, Hanton S, Denecke J (2011) Vacuolar transport in tobacco leaf epidermis cells involves a single route for soluble cargo and multiple routes for membrane cargo. Plant Cell **23**: 3007–3025

Boutté Y, Frescatada-Rosa M, Men S, Chow C-M, Ebine K, Gustavsson A, Johansson L, Ueda T, Moore I, Jürgens G, et al. (2009) Endocytosis restricts Arabidopsis KNOLLE syntaxin to the cell division plane during late cytokinesis. EMBO J **29**: 546–558

Campanoni P, Blatt MR (2007) Membrane trafficking and polar growth in root hairs and pollen tubes. J Exp Bot **58**: 65–74

Carol RJ, Dolan L (2002) Building a hair: tip growth in *Arabidopsis thaliana* root hairs. Phil Trans R Soc Lond B **357**: 815–821

Carol RJ, Takeda S, Linstead P, Durrant MC, Kakesova H, Derbyshire P, Drea S, Zarsky V, Dolan L (2005) A RhoGDP dissociation inhibitor spatially regulates growth in root hair cells. Nature **438**: 1013–1016

Chapman JM, Muhlemann JK, Gayomba SR, Muday GK (2019) RBOH-dependent ROS synthesis and ROS scavenging by plant specialized metabolites to modulate plant development and stress responses. Chem Res Toxicol **32:** 370–396

Clouse SD (2002) Arabidopsis mutants reveal multiple roles for sterols in plant development. Plant Cell **14**: 1995–2000

Cole RA, Fowler JE (2006) Polarized growth: maintaining focus on the tip. Curr Opin Plant Biol **9**: 579–588

Contento AL, Bassham DC (2012) Structure and function of endosomes in plant cells. J Cell Sci **125**: 3511–3518

Costes SV, Daelemans D, Cho EH, Dobbin Z, Pavlakis G, Lockett S (2004) Automatic and quantitative measurement of protein-protein colocalization in live cells. Biophys J **86**: 3993–4003

Denninger P, Reichelt A, Schmidt VAF, Mehlhorn DG, Asseck LY, Stanley CE, Keinath NF, Evers JF, Grefen C, Grossmann G (2019) Distinct RopGEFs successively drive polarization and outgrowth of root hairs. Curr Biol **29**: 1854–1865

Dolan L, Duckett CM, Grierson C, Linstead P, Schneider K, Lawson E, Dean C, Poethig S, Roberts K (1994) Clonal relationships and cell patterning in the root epidermis of Arabidopsis. Development **120**: 2465–2474

Foreman J, Demidchik V, Bothwell JH, Mylona P, Miedema H, Torres MA, Linstead P, Costa S, Brownlee C, Jones JD, et al. (2003) Reactive oxygen species produced by NADPH oxidase regulate plant cell growth. Nature **422**: 442–446

Geldner N, Dénervaud-Tendon V, Hyman DL, Mayer U, Stierhof YD, Chory J (2009) Rapid, combinatorial analysis of membrane compartments in intact plants with a multicolor marker set. Plant J **59**: 169–178

Grierson C, Schiefelbein J (2002) Root hairs. Arabidopsis Book **1**: e0060

Gillooly DJ, Simonsen A, Stenmark H (2001) Cellular functions of phosphatidylinositol3-phosphate and FYVE domain proteins. Biochem J **355**: 249–258

Grebe M, Xu J, Möbius W, Ueda T, Nakano A, Geuze HJ, Rook MB, Scheres B (2003) Arabidopsis sterol endocytosis involves

actin-mediated trafficking via ARA6-positive early endosomes. Curr Biol **13**: 1378–1387

Haas TJ, Sliwinski MK, Martínez DE, Preuss M, Ebine K, Ueda T, Nielsen E, Odorizzi G, Otegui MS (2007) The Arabidopsis AAA ATPase SKD1 is involved in multi vesicular endosome function and interacts with its positive regulator LYST-INTERACTING PROTEIN 5. Plant Cell **19**: 1295–1312

Hao H, Fan L, Chen T, Li R, Li X, He Q, Botella MA, Lin J (2014) Clathrin and membrane microdomains cooperatively regulate RbohD dynamics and activity in Arabidopsis. Plant Cell **26**: 1729–1745

Jones MA, Shen JJ, Fu Y, Li H, Yang Z, Grierson CS (2002) The Arabidopsis Rop2 GTPase is a positive regulator of both root hair initiation and tip growth. Plant Cell **14**: 763–776

Jones MA, Raymond MJ, Smirnoff N (2006) Analysis of the root-hair morphogenesis transcriptome reveals the molecular identity of six genes with roles in root-hair development in Arabidopsis. Plant J **45**: 83–100

Jones MA, Raymond MJ, Yang Z, Smirnoff N (2007) NADPH oxidase-dependent reactive oxygen species formation required for root hair growth depends on ROP GTPase. J Exp Bot **58**: 1261–1270

Kaya H, Takeda S, Kobayashi MJ, Kimura S, Iizuka A, Imai A, Hishinuma H, Kawarazaki T, Mori K, Yamamoto Y, et al. (2019) Comparative analysis of the reactive oxygen species-producing enzymatic activity of Arabidopsis NADPH oxidases. Plant J **98**: 291–300

Kiegle E, Gilliham M, Haselof, J, Tester M (2000) Hyperpolarisation-activated calcium channels found only in cells from the elongation zone of *Arabidopsis thaliana* roots. Plant J **21**: 225–229

Lindsey K, Pullen ML, Topping JF (2003) Importance of plant sterols in pattern formation and hormone signalling. Trends Plant Sci **8**: 521–525

Liu P, Zhang L, Li R, Wang Q, Niehaus K, Baluška F, Šamaj J, Lin J (2009) Lipid microdomain polarization is required for NADPH oxidase-dependent ROS signaling in *Picea meyeri* pollen tube tip growth. Plant J **60**: 303–313

Mangano S, Denita-Juarez SP, Choi HS, Marzol E, Hwang Y, Ranocha P, Velasquez SM, Borassi C, Barberini ML, Aptekmann AA, et al. (2017) Molecular link between auxin and ROS-mediated polar growth. Proc Natl Acad Sci USA **114**: 5289–5294

Menon AK (2002) Lipid transport - an overview. Semin Cell Dev Biol **13**: 159–162

Miedema H, Bothwell JHF, Brownlee C, Davies JM (2001) Calcium uptake by plant cells—channels and pumps acting in concert. Trends Plant Sci **11**: 514–519

Milhaud J, Hartmann MA, Bolard J (1988) Interaction of the polyene antibiotic filipin with model and natural membranes containing plant sterols. Biochim Biophys Acta **943**: 315–325

Molendijk AJ, Bischoff F, Rajendrakumar CS, Friml J, Braun M, Gilroy S, Palme K (2001) *Arabidopsis thaliana* Rop GTPases are localized to tips of root hairs and control polar growth. EMBO J **20**: 2779–2788

Monshausen GB, Bibikova TN, Messerli MA, Shi C, Gilroy S (2007) Oscillations in extracellular pH and reactive oxygen species modulate tip growth of Arabidopsis root hairs. Proc Natl Acad Sci USA **104**: 20996–21001

Morel J, Clavero S, Mongrand S, Furt F, Fromentin J, Bessoule J-J, Blein J-P, Simon-Plas F (2006) Proteomics of plant detergent-resistant membranes. Mol Cell Proteomics **5**: 1396–1411

Mukherjee S, Maxfield FR (2000) Role of membrane organization and membrane domains in endocytic lipid trafficking. Traffic **1**: 203–211

Murashige T, Skoog F (1962) A Revised Medium for Rapid Growth and Bio Assays with Tobacco Tiss Cultures. Physiol Plant **15**: 473–497

Nichols BJ, Kenworthy AK, Polishchuk RS, Lodge R, Roberts TH, Hirschberg K, Phair RD, Lippincott-Schwartz J (2001) Rapid cycling of lipid raft markers between the cell surface and Golgi complex. J Cell Biol **153**: 529–542

Ovečka M, Berson T, Beck M, Derksen J, Šamaj J, Baluška F, Lichtscheidl IK (2010) Structural sterols are involved in both the initiation and tip growth of root hairs in *Arabidopsis thaliana*. Plant Cell **22**: 2999–3019

Ovečka M, Lang I, Baluška F, Ismail A, Illéš P, Lichtscheidl IK (2005) Endocytosis and vesicle trafficking during tip growth of root hairs. Protoplasma **226**: 39–54

Ovečka M, Lichtscheidl I, Šamaj J (2014) Live microscopy analysis of endosomes and vesicles in tip-growing root hairs. Methods Mol Biol **1209**: 31–44

Ovečka M, Vaškebová L, Komis G, Luptovčiak I, Smertenko A, Šamaj J (2015) Preparation of plants for developmental and cellular imaging by light-sheet microscopy. Nat Protoc **10**: 1234–1247

Posé D, Castanedo I, Borsani O, Nieto B, Rosado A, Taconnat L, Ferrer A, Dolan L, Valpuesta V, Botella MA (2009) Identification of the Arabidopsis dry2/sqe1-5 mutant reveals a central role for sterols in drought tolerance and regulation of reactive oxygen species. Plant J **59**: 63–76

Qi X, Zheng H (2013) Rab-A1c GTPase defines a population of the trans- Golgi network that is sensitive to endosidin1 during cytokinesis in Arabidopsis. Mol Plant **6**: 847–859

Reyes FC, Buono R, Otegui MS (2011) Plant endosomal trafficking pathways. Curr Opin Plant Biol **14**: 666–673

Sagi M, Fluhr R (2006) Production of reactive oxygen species by plant NADPH oxidases. Plant Physiol **141**: 336–340

Sanderfoot AA, Kovaleva V, Bassham DC, Raikhel NV (2001) Interactions between syntaxins identify at least five SNARE complexes within the Golgi/prevacuolar system of the Arabidopsis cell. Mol Biol Cell **12**: 3733–3743

Šamaj J, Müller J, Beck M, Böhm N, Menzel D (2006) Vesicular trafficking, cytoskeleton and signalling in root hairs and pollen tubes. Trends Plant Sci **11**: 594–600

Sena F, Sotelo-Silveira M, Astrada S, Botella MA, Malacrida L, Borsani O (2017) Spectral phasor analysis reveals altered membrane order and function of root hair cells in Arabidopsis *dry2/sqe1-5* drought hypersensitive mutant. Plant Physiol Biochem **119**: 224–231

Schiefelbein JW, Somerville C (1990) Genetic control of root hair development in *Arabidopsis thaliana*. Plant Cell **2**: 235–243

Simons K, Toomre D (2000) Lipid rafts and signal transduction. Nat Rev Mol Cell Biol **1**: 31–39

Smékalová V, Luptovčiak I, Komis G, Šamajová O, Ovečka M, Doskočilová A, Takáč T, Vadovič P, Novák O, Pechan T, et al. (2014) Involvement of YODA and mitogen activated protein kinase 6 in Arabidopsis post-embryogenic root development through auxin up-regulation and cell division plane orientation. New Phytol **203**: 1175–1193

Sorek N, Gutman O, Bar E, Abu-Abied M, Feng X, Running MP, Lewinsohn E, Ori N, Sadot E, Henis YI, et al. (2011) Differential effects of prenylation and S-acylation on type I and II ROPS membrane interaction and function. Plant Physiol **155**: 706–720

Sorek N, Poraty L, Sternberg H, Buriakovsky E, Bar E, Lewinsohn E, Yalovsky S (2017) Activation status coupled transient S-acylation determines membrane partitioning of a plant Rho-related GTPase. Mol Cell Biol **37**: 2144–2154

Srivastava V, Malm E, Sundqvist G, Bulone V (2013) Quantitative proteomics reveals that plasma membrane microdomains from poplar cell suspension cultures are enriched in markers of signal transduction, molecular transport, and callose biosynthesis. Mol Cell Proteomics **12**: 3874–3885

Stanislas T, Hüser A, Barbosa IC, Kiefer CS, Brackmann K, Pietra S, Gustavsson A, Zourelidou M, Schwechheimer C, Grebe M (2015) Arabidopsis D6PK is a lipid domain-dependent mediator of root epidermal planar polarity. Nat Plants **1**: 15162

Takeda S, Gapper C, Kaya H, Bell E, Kuchitsu K, Dolan L (2008) Local positive feedback regulation determines cell shape in root hair cells. Science **319**: 1241–1244

Torres MA, Dangl JL, Jones JD (2002) Arabidopsis gp91phox homologues AtrbohD and AtrbohF are required for accumulation of reactive oxygen intermediates in the plant defence response. Proc Natl Acad Sci USA **99**: 517–522

Ueda T, Uemura T, Sato MH, Nakano A (2004) Functional differentiation of endosomes in Arabidopsis cells. Plant J **40**: 783–789

Uemura T, Ueda T, Ohniwa RL, Nakano A, Takeyasu K, Sato MH (2004) Systematic analysis of SNARE molecules in Arabidopsis: dissection of the post-Golgi network in plant cells. Cell Struct Func **29**: 49–65

Véry AA, Davies JM (2000) Hyperpolarization-activated calcium channels at the tip of Arabidopsis root hairs. Proc Natl Acad Sci USA **97**: 9801–9806

Viotti C, Bubeck J, Stierhof YD, Krebs M, Langhans M, van den Berg W, van Dongen W, Richter S, Geldner N, Takano J, et al. (2010) Endocytic and secretory traffic in Arabidopsis merge in the trans- Golgi network/early endosome, an independent and highly dynamic organelle. Plant Cell **22**: 1344–1357

Voigt B, Timmers A, Šamaj J, Hlavacka A, Ueda T, Preuss M, Nielsen E, Mathur J, Emans N, Stenmark H, et al. (2005) Actin-based motility of endosomes is linked to the polar tip growth of root hairs. Eur J Cell Biol **84**: 609–621

von Wangenheim D, Rosero A, Komis G, Šamajová O, Ovečka M, Voigt B, Šamaj J (2016) Endosomal interactions during root hair growth. Front Plant Sci **6**: 1262

Wachtler V, Rajagopalan S, Balasubramanian MK (2003) Sterol-rich plasma membrane domains in the fission yeast *Schizosaccharomyces pombe*. J Cell Sci **116**: 867–874

Wymer CL, Bibikova TN, Gilroy S (1997) Cytoplasmic free calcium distributions during the development of root hairs of *Arabidopsis thaliana*. Plant J **12**: 427–439

Zhou X, Xiang Y, Li C, Yu G (2020) Modulatory role of reactive oxygen species in root development in model plant of *Arabidopsis thaliana*. Front Plant Sci **11**: 485932